Development/Plasticity/Repair

Spatial Mapping of Activity Changes across Sensory Areas Following Visual Deprivation in Adults

Samuel Parkins,[1,2*] Yidong Song,[1*] Yanis Jaoui,[1] Aryan Gala,[1] Kaven T. Konda,[1,2] Crispo Richardson,[1] and Hey-Kyoung Lee[1,2,3,4]

[1]Zanvyl-Krieger Mind/Brain Institute, Johns Hopkins University, Baltimore, Maryland 21218, [2]Cell Molecular Developmental Biology and Biophysics Graduate Program, Johns Hopkins University, Baltimore, Maryland 21218, [3]Solomon H. Snyder Department of Neuroscience, Johns Hopkins School of Medicine, Baltimore, Maryland 21205, and [4]Kavli Neuroscience Discovery Institute, Johns Hopkins University, Baltimore, Maryland 21218

Loss of a sensory modality triggers global adaptation across brain areas, allowing the remaining senses to guide behavior more effectively. There are specific synaptic and circuit plasticity observed across many sensory areas, which suggests potential widespread changes in activity. Here we used a cFosTRAP2 mouse line to drive tdTomato (tdT) expression in active cells to spatially map the extent of activity changes in various sensory areas in adult mice of both sexes following two modes of visual deprivation. We found that in the primary visual cortex (V1), both dark exposure (DE) and enucleation (EN) caused an initial loss of active cells followed by a partial rebound, which occurred relatively more in the superficial layers. A similar pattern was observed in the secondary visual cortex, especially in the lateral areas (V2L). The spared primary sensory cortices adapted distinctly. In the primary somatosensory barrel cortex (S1BF), there was a change in the density of active cells dependent on the duration and the mode of visual deprivation. In the primary auditory cortex (A1), there was a relative reduction in the density of active cells in the superficial layers without a significant change in the overall density. There were minimal changes in the active cell density in the secondary cortices of the spared senses and the multisensory retrosplenial cortex (RSP). Our results are consistent with cross-modal recruitment of the deprived visual cortex and compensatory plasticity in the spared primary sensory cortices that can support enhanced processing and refinement of the spared senses.

Key words: **cFosTRAP2; compensatory plasticity; cortical plasticity; cross-modal plasticity; sensory cortex; vision loss**

Significance Statement

The neural basis for improved processing of the spared senses after losing vision is largely dependent on plasticity mechanisms driven by neural activity. Using a transgenic mouse model to label active neurons in a temporally controlled manner, this study reveals the spatial pattern of widespread activity changes across brain areas following visual deprivation in adult mice. The findings suggest that the deprived visual cortex undergoes an initial reduction in activity followed by a rebound suggestive of cross-modal recruitment. Activity changes in the spared primary sensory cortices conform to compensatory plasticity, which could support improved processing of the spared senses. The results highlight the presence of large-scale plasticity in the adult brain to compensate for loss of vision.

Introduction

Vision loss leads to widespread adaptation across brain areas to allow functional compensation as evident from the ability of blind individuals to more effectively use the remaining senses to guide behavior (Bavelier and Neville, 2002; Park and Fine, 2024). A large body of evidence supports the idea that vision loss triggers plasticity across different sensory cortices, which can be categorized into plasticity in the deprived sensory areas to mediate cross-modal recruitment and compensatory plasticity in the spared sensory cortices (Ewall et al., 2021; Mesik and Lee, 2023). Examples of cross-modal recruitment are activation of the deprived visual cortex upon braille reading or speech in both early- and late-onset blind humans (Sadato et al., 1996; Buchel et al., 1998; Roder et al., 2002; Bedny et al., 2015). Furthermore, normal adults with blindfolds show an advantage in learning braille characters than sighted cohorts dependent on activity in the visual cortex (Merabet et al., 2008) suggesting that cross-modal recruitment may occur quite rapidly in the adult brain. Compensatory plasticity has also been observed in blind humans as a functional expansion of the representation of the braille

Received May 21, 2024; revised Oct. 22, 2024; accepted Nov. 14, 2024.

Author contributions: S.P. and H.-K.L. designed research; S.P., Y.S., Y.J., A.G., K.T.K., and C.R. performed research; Y.S. contributed unpublished reagents/analytic tools; S.P., Y.S., K.T.K., and H-K.L. analyzed data; H.-K.L. wrote the paper.

This work was supported by National Institutes of Health Grant R01-EY014882 to H.-K.L and F31-EY031946 to S.P.

*S.P. and Y.S. contributed equally to this work and are the first authors.

The authors declare no competing financial interests.

Correspondence should be addressed to Hey-Kyoung Lee at heykyounglee@jhu.edu.

https://doi.org/10.1523/JNEUROSCI.0969-24.2024

reading finger (Pascual-Leone and Torres, 1993) and auditory cortical areas (Elbert et al., 2002), as well as refinement of tonotopy in the primary auditory cortex (Huber et al., 2019).

Animal models have been useful in elucidating the cellular and circuit mechanisms of cross-modal plasticity. Depriving vision of adult mice for a few days leads to widespread synaptic plasticity across the primary sensory cortical areas. In the deprived V1, there is a rather selective potentiation of synapses serving the lateral intracortical inputs to layers 2/3 (L2/3) without changes in the strength of synapses that provide feedforward information (Petrus et al., 2014, 2015; Chokshi et al., 2019). These synaptic changes are consistent with the idea that vision loss would enhance the impact of contextual information arriving in V1 through long-range connections from other brain areas to serve cross-modal recruitment (Ewall et al., 2021; Mesik and Lee, 2023). In the spared primary sensory cortices, several days of vision loss leads to a different type of adaptation, which manifests primarily as potentiation of feedforward synapses in both the primary somatosensory barrel field (S1BF) and the primary auditory cortex (A1; Jitsuki et al., 2011; Petrus et al., 2014, 2015). Such plasticity could mediate increased sensitivity to spared sensory inputs, which has been observed as a decrease in the threshold of A1 L4 neurons to sound stimuli in visually deprived adult mice (Petrus et al., 2014). There is also data supporting the functional refinement of cortical circuitry within A1 and S1BF of visually deprived mice (Jitsuki et al., 2011; Meng et al., 2015, 2017; Solarana et al., 2019). The observed functional circuit plasticity suggests changes in neural activity across the sensory areas in response to vision loss.

Immediate early genes (IEGs) have been used widely as reporters of neural activity, in particular, IEGs such as c-*fos*, exhibit rapid and transient activation ideal for detecting changes in activity (Flavell and Greenberg, 2008). Furthermore, c-*fos* expression is triggered by induction of long-term potentiation (LTP; Dragunow et al., 1989; Nikolaev et al., 1991; Kaczmarek, 1992), which suggests its utility as a marker for high activity conducive to plasticity. In this study, to determine the spatial extent of neural activity changes accompanying visual deprivation, we utilized the cFos-Targeted Recombination in Active Populations 2 (cFosTRAP2) mouse line (DeNardo et al., 2019), which when crossed with a reporter line allows permanent labeling of active neurons at the time of tamoxifen injection. We found that two different modes of visual deprivation, dark exposure (DE) and enucleation (EN), which induce cross-modal synaptic plasticity across sensory cortices (Goel et al., 2006; He et al., 2012; Petrus et al., 2014, 2015; Rodriguez et al., 2018), produce similar but distinct changes in the spatial pattern of cFosTRAP2-labeled active neurons across sensory cortices.

Materials and Methods

Animals. All animal handling and manipulations were approved by the Institutional Animal Care and Use Committee (IACUC) at Johns Hopkins University. Animals were housed under a normal light/dark cycle (12 h light/dark) until they reached the required age range for experiments [postnatal day (P) 90–120]. cFosTRAP2 [Fos tm2.1(icre/ERT2)Luo/J, Jax stock # 030323, RRID:IMSR_JAX:030323; DeNardo et al., 2019] were crossed with Ai14 [B6.Cg-Gt(ROSA)26Sor tm14(CAG-tdTomato)Hze/J, Jax stock # 007914, RRID: IMSR_JAX:007914] to generate the cFos-TRAP2;Ai14 transgenic line. Mice of both sexes were used for all experiments.

Induction of tdT in active neurons. Labeling of active cortical neurons was done by intraperitoneal injection of a tamoxifen analog, 4-hydroxytamoxifen (4-OHT; 50 μg/g of body weight), to cFos-TRAP2;Ai14 mice. 4-OHT was prepared as in our published study (Mesik et al., 2024). Injection time was matched across the cohorts and was between Zeitgeber time (ZT) 10 to 12. Mice were then left for a week to allow for sufficient expression of tdT before being prepared for perfusion and histology. We previously verified that the cFos-TRAP2;Ai14 line shows negligible background leakage of tdT expression without 4-OHT injection, and injection of 4-OHT allows sufficient induction of tdT expression 1 week after sensory experience (Mesik et al., 2024).

Dark exposure. Mice aged between P90 and P120 were randomly split into the control (normal reared, NR: three males and three females), 2 d dark-exposed (2dDE: three males and three females), and 7 d dark-exposed (7dDE: three males and two females) groups. The mice in the dark-exposed groups were placed in a light-tight dark room and were cared for using infrared goggles (NIGHTFOX Red HD Digital Night Vision Goggles, model NF-RED). After 2 d (2dDE group) or 7 d (7dDE group), the mice were given an intraperitoneal injection of 4-OHT to initiate Cre-mediated recombination and kept in the dark-room for a further week to allow sufficient expression of tdT. DE mice were singly housed during the time in the darkroom to avoid misidentification in the dark and to allow proper dosing of tamoxifen based on measured body weight. In a second set of experiments, DE mice were group housed for 7 d in the dark (7dDEg, three females) to control for potential effects of social isolation. To distinguish each mouse in the dark using infrared goggles, the fur was dyed with distinct patterns using the Clairol Nice'N Easy Blonde Hair dye. A cohort of age-matched NR controls (two females) were also dyed with a pattern to match the handling.

Binocular enucleation. Mice (P90–P120) were anesthetized using isoflurane (5% induction, 2% maintenance) and mounted on a stereotaxic apparatus (Kopf) without the use of ear bars. To gain access to the eyes more easily, the head was rotated sideways, and the eye was extracted out of the socket using curved tweezers. The eye was then grabbed at the base by the optic nerve, twisted around at least three times to prevent bleeding and cutoff using surgical scissors. Finally, eyelids were glued together using tissue adhesive (Vetbond). After recovery, the mice were placed back in normal light/dark cycle and given an intraperitoneal injection of 4-OHT at 2 or 7 d after binocular enucleation (2dEN or 7dEN groups, respectively; 2dEN, two males and four females; 7dEN, four males and five females) to induce Cre-mediated recombination and kept for a further week to allow sufficient expression of tdT. Mice were then perfused, and their brains were prepared for histology.

Histological analysis of cFos-TRAP2;Ai14 neurons. A week after tamoxifen injection, mice were deeply anesthetized using isoflurane vapors. The absence of toe pinch and corneal reflex were used as indicators of the depth of anesthesia. Mice were kept under isoflurane anesthesia during the perfusion using a nose cone and transcardially perfused with ~10 ml of phosphate-buffered saline (PBS), pH 7.4, followed by ~10 ml of 10% formalin solution (Sigma-Aldrich, catalog #HT5012). Mice were then decapitated, and their brains were extracted and placed in formalin solution at 4̊C overnight to be postfixed. A vibratome (Vibratome 1000 Plus, Ted Pella) was used to make 100-μm-thick coronal sections from the postfixed brains. Seven sections were selected per mouse (Table 1) that spanned anterior to posterior regions of the brain intending to match these sections across all animals. The sections were counterstained with DAPI (1:1,000), mounted, coverslipped with ProLong

Table 1. Atlas plates corresponding to brain sections imaged

Plate	Displacement from interaural line (mm)	Displacement from bregma (mm)
39	2.86	−0.94
45	2.10	−1.70
48	1.74	−2.06
51	1.34	−2.46
55	0.88	−2.92
58	0.52	−3.28
63	−0.88	−3.88

Atlas plate numbers are from *The Mouse Brain in Stereotaxic Coordinates, Second Edition* (Paxinos and Franklin, 2001).

Antifade mounting media (Thermo Fisher Scientific), nail polish sealed, and stored in a light-tight slide box. The slides were imaged on a confocal microscope (LSM 700, Zeiss) using the 10× objective. Tiled images were taken of either the whole brain section or separately for each hemisphere at a frame size of 1,024 × 1,024 pixels and stitched together using the tile function. Confocal imaging settings were kept the same across all imaging sessions. Image analysis, described below, was done using custom scripts in QuPath (Bankhead et al., 2017) and MATLAB (MathWorks) after registering the brain sections to the Allen Mouse Brain Common Coordinate Framework (CCF; see details below).

cFos-TRAP2;Ai14 cell density analysis. Images for analysis were converted to 8 bit .tiff files using FIJI (Schindelin et al., 2012). Using QuPath (Bankhead et al., 2017), a project was made for the slices corresponding to a single mouse. The QuPath project was then imported into the ImageJ plugin Aligning Big Brains & Atlases (ABBA; https://biop.github.io/ijp-imagetoatlas/), which employs the Allen Brain Atlas V3p1 for the adult mouse brain. The interactive transform tool was used to register the coronal sections to the best matching atlas plates, and the registered slices with annotated brain areas (regions of interest, ROIs) were exported back to QuPath. Using the registrations, ROIs were loaded onto the images as annotations and manually adjusted. The parameters to detect the tdT-positive (tdT^+) cells were set as threshold = 80, minimum area = 40 μm^2, maximum area = 400 μm^2, and sigma = 1.5. The cell detection script was run, and the number and x–y coordinates of cells within each region were exported along with the area of the regions. The number of cells and the area of each region were used to calculate the density per region. The custom scripts used were generated by Y. Song (https://github.com/heykyounglee/QuPathScripts_CellDensity_CellDepth).

Cell depth profile analysis. In a separate QuPath project, the pia of the coronal sections was labeled with points. The x–y coordinates for these points were exported, and using a custom MATLAB (MathWorks) script (https://github.com/heykyounglee/CellDepthAnalysisWithROI), the linear distance of each cell from the pia was calculated. Fractions of cells were binned into 100 μm distances from the pia surface for each group. This value was multiplied by the median density of tdT^+ cells of each group to generate the tdT^+ cell density across the depth from pia plots. In addition, relative fractions of cells per 100 μm depth were calculated for each section to statistically determine a relative shift in the distribution of tdT^+ cells across the depth.

Behavioral analysis. To monitor potential behavioral changes as a result of visual deprivation, cFosTRAP2;Ai14 mice were randomly split into two groups: DE (four males and five females) and EN (four males and four females). Mice were video recorded in their home cage a day prior (−1 d, NR) to visual deprivation and afterward at 2 and 7 d (2dDE/2dEN and 7dDE/7dEN). DE mice were housed singly the day prior and for the duration of DE to be consistent with the conditions used for labeling active cells. To track the group-housed mice in the EN groups across multiple days, some were randomly selected to have their fur dyed with a pattern for identification. Each video recording was done using a camera mounted above the cage without the lid. The video camera used for monitoring DE mice (KJK Trail Camera, model KJK-LCK228) operates wirelessly on a rechargeable battery and has a built-in infrared light (950 nm wavelength) for capturing images in complete darkness without any potential for light exposure. The camera has a small visible LED light, which was occluded. EN mice were monitored using a wired video camera (Green Backyard HD Bird camera kit; model 4946-09). Recordings were performed for 1 h during the same time window (ZT10–ZT12) in which the mice used in the tdT^+ cell density measurements were injected with 4-OHT for trapping activity. Behavioral analysis was manually scored using Behavioral Observation Research Interactive Software (BORIS; Friard and Gamba, 2016).

Experimental design and statistical analysis

Experimental design was done to allow statistical comparison between NR, 2dDE, 7dDE, 2dEN, and 7dEN groups. All statistical analyses were done using Prism (GraphPad) and R (https://www.r-project.org) programs. Most of the datasets on cell density measurement were not normally distributed (Shapiro–Wilk test: $p > 0.05$); hence the Aligned Rank Transform (ART) for nonparametric factorial data analysis (Wobbrock et al., 2011) was done using the ARTool package (v.2.1.2) for R (https://cran.r-project.org/web/packages/ARTool/index.html). Cell density in each ROI per brain section was taken as a data point (n). Outliers were removed from the final dataset using the robust regression and outlier removal (ROUT) method with the ROUT coefficient (Q) = 1%. Most of the data displayed clustering effect due to animal-to-animal variability as determined by the intra-class correlation (ICC $= \frac{\sigma_b^2}{\sigma_b^2+\sigma_e^2}$, where σ_b^2 is the between-class variance and σ_e^2 is the within-class variance) > 0.4. The clustering effect was taken into consideration for statistical analysis by setting the animal as a random effects variable in the linear mixed effects (LME) model within the ARTool. For datasets with $p < 0.05$ from the LME model nonparametric one-way ANOVA (ARTool), pairwise comparisons were made to determine the differences between experimental groups using post hoc tests in the ARTool. Cell density data are presented in box and whisker plots, where the box outlines 25 and 75% of ranges with a line inside that correspond to the median value and the whiskers show the full range of data (minimum and maximum values). For comparisons of the depth profile of relative fractions of tdT^+ cells, two-way ANOVA was used to determine the interaction between experimental groups and depth from pia. For cortical areas that showed significant interactions (p value < 0.05), Tukey's multiple-comparisons post hoc test was used to determine at which depths there were significant differences in the relative fraction of tdT^+ cells across the experimental groups. For comparing each category of behavior for DE and EN groups before and after visual deprivation, two-way ANOVA was used to determine the interaction between the sensory manipulation across different days. A p value < 0.05 was used as the measure of statistical significance. Specific statistical analyses and exact p values are detailed in each figure legend. Final datasets are available on the Mendeley Data (https://DOI.ORG/10.17632/dgv8jrxt4w.1).

Code accessibility

Custom-made analysis codes are publicly available through GitHub (www.github.com) with the links provided above.

Results

The main goal of this study was to determine the spatial extent of changes in active neurons across various sensory cortical areas following visual deprivation. To determine the spatial extent of neural activity changes, we used the cFosTRAP2;Ai14 mouse line (Fig. 1*A*), which expresses tdT in active neurons within a 6 h window around the time of 4-OHT injection (DeNardo et al., 2019). Two different modes of visual deprivation were used: dark exposure (DE), which removed all visual inputs while the retina remained intact, and enucleation (EN), where both eyes were surgically removed. The former models vision loss without physical damage and leaves spontaneous retinal activity intact, while the latter models retinae and optic nerve damage. Visual deprivations were done for 2 and 7 d to determine whether the duration of vision loss alters the outcome of neural activity adaptation. We previously reported minimal leakage of tdT expression in the absence of 4-OHT and induction of tdT in ipsilateral visual areas upon monocular deprivation (Mesik et al., 2024). However, we observed that the model was not robust

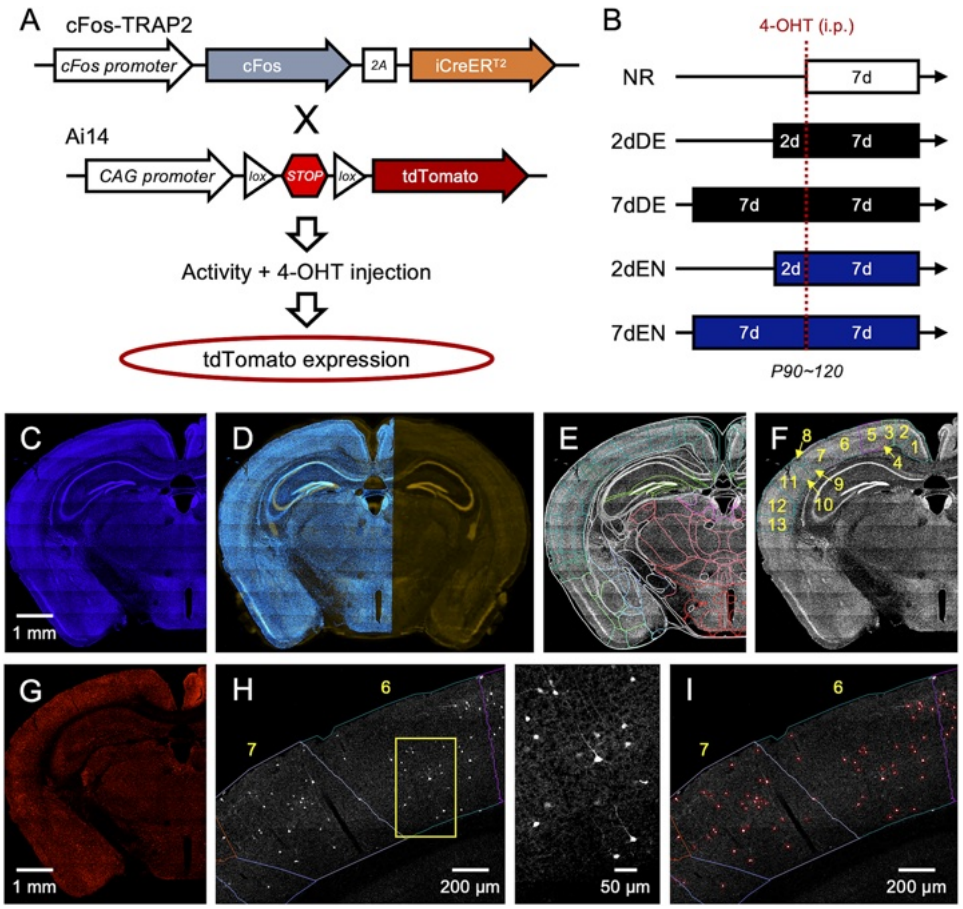

Figure 1. Using cFosTRAP2;Ai14 mice for spatial mapping of active neurons with visual deprivation. ***A***, Schematics of cFosTRAP2;Ai14. cFosTRAP2 mice were crossed with Ai14 to generate cFosTRAP2;Ai14, which allows expression of tdT in active neurons at the time of intraperitoneal (i.p.) injection of 4-OHT. ***B***, Schematics of the experimental groups. Adult mice were divided into five groups: A control normal reared (NR) group kept in a normal light/dark cycle, dark-exposed (DE) groups kept in a light-tight darkroom 2 d (2dDE) or 7 d (7dDE) prior to 4-OHT injection, and binocular enucleation (EN) groups, which were enucleated either 2 d (2dEN) or 7 d (7dEN) prior to 4-OHT injection. Brains were collected 7 d after 4-OHT injection, sectioned, counterstained with DAPI, and processed for histology. ***C–I***, Image analysis pipeline using QuPath and ABBA image analysis programs. See Materials and Methods for details. ***C***, An example of a tiled confocal image (taken using a 10× objective lens) of DAPI-stained coronal section used for the alignment. This example is from a NR mouse. ***D***, DAPI-stained image section was imported into the ABBA software and aligned to the Allen Brain Atlas V3p1 for the adult mouse brain. ***E***, Brain area boundaries from the Allen Brain Atlas are overlaid on the DAPI image section. ***F***, Cortical regions of interest (ROIs) were selected from the area outlines and the boundaries were further adjusted to match the image section. Annotations: 1, RSPv (retrosplenial area, ventral part); 2, RSPd (retrosplenial area, dorsal part); 3, RSPagl (retrosplenial area, lateral agranular part); 4, VISpm (posteriomedial visual area); 5, VISam (anteromedial visual area); 6, VISp (primary visual area); 7, VISrl (rostrolateral visual area); 8, VISal (anterolateral visual area); 9, SSp-bfd (primary somatosensory area, barrel field); 10, SSs (supplemental somatosensory area); 11, AUDd (dorsal auditory area); 12, AUDp (primary auditory area); 13, AUDv (ventral auditory area). ***G***, An image of the corresponding tdT channel is shown. ***H***, Selected ROIs are overlaid on the tdT image section. ROI numbers correspond to labels in panel ***F***. The right panel shows the zoomed-in image corresponding to the yellow outlined box in the left panel. Note tdT^+ cortical cells. ***I***, tdT^+ cells are selected (shown with red outlines) using the QuPath software for quantification of cell density and depth from pia as detailed in the Materials and Methods. ROI numbers correspond to labels in panel ***F***.

in inducing tdT in subcortical regions (Mesik et al., 2024), hence here we mainly focused our analyses on cortical areas.

To label the active neurons with tdT as a fluorescent marker, we injected 4-OHT into five groups of adult mice (P90~120; Fig. 1*B*): A group of normal reared (NR) mice, which were kept in 12 h light/dark cycle, two groups of mice that were placed in complete darkness (dark exposed, DE) for 2 d (2dDE) or 7 d (7dDE) prior to the 4-OHT injection, and two groups of mice that underwent enucleation (EN) for 2 d (2dEN) or 7 d (7dEN) prior to the 4-OHT injection. Mice were kept for an additional 7 d, which is needed to produce sufficient tdT expression for visualization of active neurons around the time of 4-OHT injection (DeNardo et al., 2019), before the brains were fixed and sectioned for imaging. We selected seven sections from each brain to roughly correspond to similar coronal section planes (see Table 1 for details) to allow imaging of relevant cortical areas. Using the DAPI counterstain images, we aligned each half hemisphere confocal images (tile scanned) to the Allen Brain Atlas for the adult mouse brain using the ABBA software to delineate the borders of each cortical area of interest (see Materials and Methods for details; Fig. 1*C–F*). We focused our analysis on primary sensory cortical areas (primary visual, somatosensory, and auditory cortices), secondary sensory cortical areas (secondary visual, somatosensory, and auditory cortices), and the retrosplenial cortex (RSP) as a representative multisensory cortical area. Active cells labeled by tdT were selected using the QuPath image analysis software (see Materials and Methods for details; Fig. 1*G–I*). The density of labeled cells was calculated for each cortical area and the depth of each cell from pia was analyzed for each area of interest. Example image plates from each experimental group are shown in Figure 2*A*. We found that almost all of the tdT-positive (tdT^+) cells in the cortex are neurons, as observed by double labeling with a neuronal marker, NeuN (Fig. 2*B*).

Differences in active cell density across the brain areas in normal controls

We analyzed tdT$^+$ cell density across 18 brain areas, including sensory cortices and sensory thalamic nuclei (Fig. 2*C*). Secondary visual areas were grouped into ones that are located lateral (V2L) and medial (V2M) to V1 for analysis. The primary somatosensory cortex was divided into barrel fields (S1BF) and other S1 areas (S1 other) for evaluation. Subdivisions of the retrosplenial cortex (RSP) were grouped for analysis. We compared the tdT$^+$ cell density across the 18 areas in normal reared (NR) controls and found significant differences across areas (Fig. 2*C*, Table 2). In general, the cortical areas showed significantly higher density of tdT$^+$ cells compared with thalamic areas. The ventral lateral geniculate nucleus (vLGN), which is largely composed of GABAergic neurons (Harrington, 1997; Inamura et al., 2011; Sabbagh et al., 2021) and is part of a nonimaging forming visual pathway (Hattar et al., 2002; Lazzerini Ospri et al., 2017), was an exception with the highest density of tdT$^+$ cells among the thalamic nuclei, quite comparable with the cortical areas. The visual cortical areas (V1, V2L, and V2M) showed significantly higher densities of tdT$^+$ cells compared with all other regions. S1BF showed higher density compared with S1 other and the secondary somatosensory cortex (S2). The primary auditory cortex (A1) and RSP had a similar density of tdT$^+$ cells as in S1BF. Most

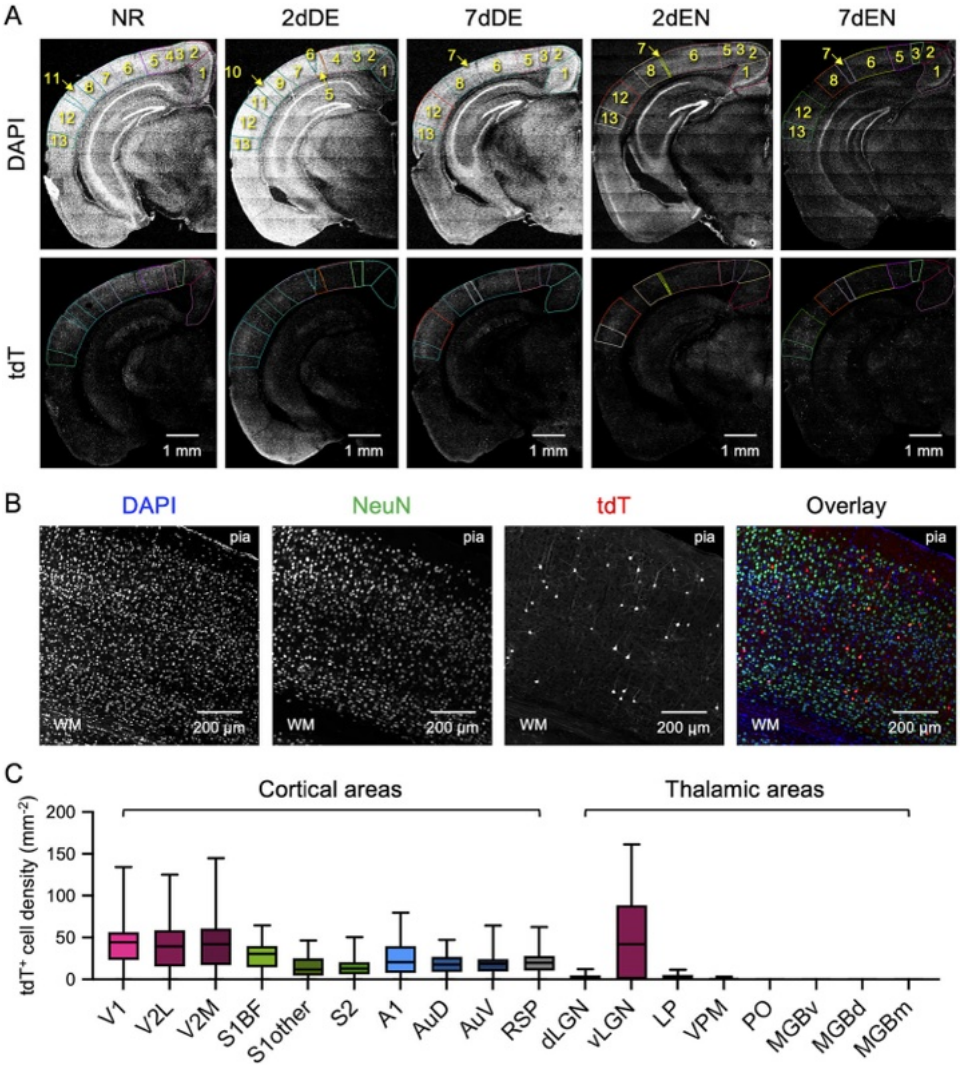

Figure 2. Example coronal section images from each experimental group. ***A***, Coronal image sections from each experimental group were selected to correspond to plate 55 of the Mouse Brain Stereotaxic Coordinates (Paxinos and Franklin, 2001; see Table 1 for coordinates). Top rows, DAPI-stained images. Bottom rows, tdT images. Outlined area boundaries are ROIs matched to the Allen Brain Atlas for adult mouse brains. ROI numbers are the same as listed in Figure 1*F* legend. ***B***, tdT$^+$ cortical cells are mostly neurons. Confocal tiled image (20× objective lens) of a cortical brain section stained with a neuronal marker NeuN. First panel, DAPI counterstain. Second panel, NeuN staining. Third panel, tdT imaging. Fourth panel, Overlay (blue, DAPI; green, NeuN; red, tdT). ***C***, Comparison of tdT$^+$ cells from NR controls across the brain areas examined in this study. Visual areas are colored in spectrums of red, somatosensory areas are in spectrums of green, auditory areas are in spectrums of blue, and a multisensory area (retrosplenial cortex, RSP) is shown in gray. Visual areas have a significantly higher density of tdT expression compared with other sensory areas. Thalamic areas display very low tdT$^+$ cell density compared with cortical areas, except the ventral LGN (vLGN), which largely contains GABAergic neurons. Data values plotted in the graph are noted under subsequent figure legends for each brain area. LME model nonparametric one-way ANOVA test (ARTool): $F_{(17,615.633)} = 62.536$, $p < 0.0001$. Pairwise-comparisons post hoc test p values are compiled in Table 2. Abbreviations: V1, primary visual cortex; V2L, lateral areas of the secondary visual cortex; V2M, medial areas of the secondary visual cortex; S1BF, primary somatosensory cortex barrel fields; S1other, primary somatosensory cortex other than the barrel fields; S2, secondary somatosensory cortex; A1, primary auditory cortex; AuD, dorsal secondary auditory cortex; AuV, ventral secondary auditory cortex; RSP, retrosplenial cortex; dLGN, dorsal lateral geniculate nucleus; vLGN, ventral lateral geniculate nucleus; LP, lateral posterior thalamic nucleus; VPM, ventral posteromedial thalamic nucleus; PO, posterior thalamic nuclear group; MGBv, ventral portion of the medial geniculate body; MGBd, dorsal portion of the medial geniculate body; MGBm, medial portion of the medial geniculate body.

Table 2. Pairwise comparisons of tdT$^+$ cell density across areas shown in Figure 2C

	V1	V2L	V2M	S1BF	S1other	S2	A1	AuD	AuV	RSP	dLGN	vLGN	LP	VPM	PO	MGBv	MGBd	MGBm
V1	–	0.193	0.428	<0.001	<0.001	<0.001	<0.001	<0.001	<0.001	<0.001	<0.001	<0.001	<0.001	<0.001	<0.001	<0.001	<0.001	<0.001
V2L	–	–	0.566	0.0187	<0.001	<0.001	<0.001	<0.001	<0.001	<0.001	<0.001	0.0169	<0.001	<0.001	<0.001	<0.001	<0.001	<0.001
V2M	–	–	–	0.0037	<0.001	<0.001	<0.001	<0.001	<0.001	<0.001	<0.001	0.0031	<0.001	<0.001	<0.001	<0.001	<0.001	<0.001
S1BF	–	–	–	–	<0.001	<0.001	0.284	0.025	0.043	0.094	<0.001	0.971	<0.001	<0.001	<0.001	<0.001	<0.001	<0.001
S1other	–	–	–	–	–	0.669	0.0056	0.072	0.028	0.0063	<0.001	<0.001	<0.001	<0.001	<0.001	<0.001	<0.001	<0.001
S2	–	–	–	–	–	–	0.005	0.096	0.029	0.0039	<0.001	<0.001	<0.001	<0.001	<0.001	<0.001	<0.001	<0.001
A1	–	–	–	–	–	–	–	0.245	0.387	0.677	<0.001	0.258	<0.001	<0.001	<0.001	<0.001	<0.001	<0.001
AuD	–	–	–	–	–	–	–	–	0.699	0.345	<0.001	0.02	<0.001	<0.001	<0.001	<0.001	<0.001	<0.001
AuV	–	–	–	–	–	–	–	–	–	0.565	<0.001	0.034	<0.001	<0.001	<0.001	<0.001	<0.001	<0.001
RSP	–	–	–	–	–	–	–	–	–	–	<0.001	0.075	<0.001	<0.001	<0.001	<0.001	<0.001	<0.001
dLGN	–	–	–	–	–	–	–	–	–	–	–	<0.001	0.885	0.073	0.025	0.081	0.075	0.028
vLGN	–	–	–	–	–	–	–	–	–	–	–	–	<0.001	<0.001	<0.001	<0.001	<0.001	<0.001
LP	–	–	–	–	–	–	–	–	–	–	–	–	–	0.086	0.03	0.095	0.087	0.033
VPM	–	–	–	–	–	–	–	–	–	–	–	–	–	–	0.654	0.846	0.816	0.579
PO	–	–	–	–	–	–	–	–	–	–	–	–	–	–	–	0.84	0.869	0.889
MGBv	–	–	–	–	–	–	–	–	–	–	–	–	–	–	–	–	0.973	0.753
MGBd	–	–	–	–	–	–	–	–	–	–	–	–	–	–	–	–	–	0.779
MGBm	–	–	–	–	–	–	–	–	–	–	–	–	–	–	–	–	–	–

p values are listed for each pair. Statistically significant values are colored in different shades of gray from $0.01 \leq p < 0.05$ being the lightest shade followed by $0.005 \leq p < 0.01$, $0.001 \leq p < 0.005$, and $p < 0.001$ being the darkest. Unshaded pairs are not statistically significant ($p \geq 0.05$). Cells denoted with "–" are not compared.

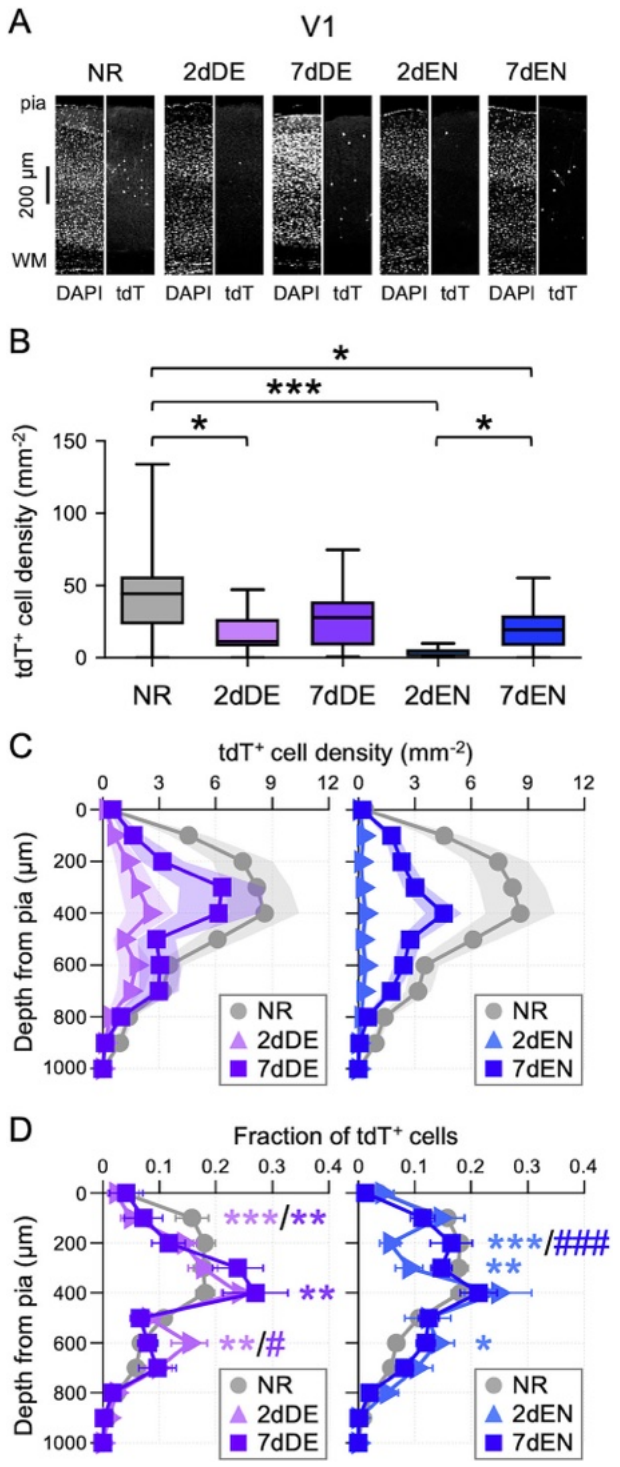

Figure 3. In V1, both DE and EN decrease the density of tdT^+ cells followed by a partial rebound after 7 d with a relatively greater reduction in superficial depths. ***A***, Example images of V1 sections across groups. Both DAPI and tdT images are shown side by side as labeled for NR, 2dDE, 7dDE, 2dEN, and 7dEN. Tiled confocal images taken at 10× were cropped and rotated to align the pia and white matter (WM) for display. ***B***, Quantification of tdT^+ cell density in V1 across groups displayed as box and whisker plot. Median value with interquartile range (IQR): NR = 44.3 (IQR 23.6–56.2) mm^{-2}, $n = 40$ sections from six mice; 2dDE = 11.4 (IQR 7.8–20.1) mm^{-2}, $n = 24$ sections from four mice; 7dDE = 27.7 (IQR 14.1–39.1) mm^{-2}, $n = 17$ sections from four mice; 2dEN = 2.1 (IQR 1.0–5.9) mm^{-2}, $n = 36$ sections from seven mice; 7dEN = 19.3 (IQR 8.3–29.2) mm^{-2}, $n = 43$ sections from eight mice. LME model nonparametric one-way ANOVA test (ARTool): $F_{(4,23.98)} = 4.8787$, $p = 0.0051$. Pairwise-comparisons post hoc test: $^*p < 0.05$ and $^{***}p < 0.005$. ***C***, Depth profile of tdT^+ cell density in each group normalized to the respective median density shown in panel ***B***. Shaded areas outline 95% confidence intervals. Left graph, Comparison of NR, 2dDE, and 7dDE groups. Right graph, Comparison of NR, 2dEN, and 7dEN groups. ***D***, Relative fraction of tdT^+ cells across the depth of V1. Left graph, Comparison of NR, 2dDE, and 7dDE groups. Two-way ANOVA: Interaction between group and depth, $F_{(24,936)} = 2.496$, $p < 0.0001$. Tukey's multiple-comparison post hoc test, * or $^{\#}p < 0.05$, $^{**}p < 0.01$, $^{***}p < 0.005$ (light purple asterisks, between NR and 2dDE; dark purple asterisks, between NR and 7dDE; dark purple hashtags, between 2dDE and 7dDE). Right graph, Comparison of NR, 2dEN, and 7dEN groups. Two-way ANOVA: Interaction between group and depth, $F_{(24,1300)} = 2.052$, $p = 0.002$. Tukey's multiple-comparison post hoc test, * or $^{\#}p < 0.05$, ** $p < 0.01$, *** or $^{\#\#\#}p < 0.005$ (light blue asterisks, between NR and 2dEN; dark blue hashtags, between 2dEN and 7dEN). Average ± SEM values are plotted. Symbols: NR, gray circles; 2dDE, light purple triangles; 7dDE, dark purple squares; 2dEN, light blue triangles; 7dEN, dark blue squares.

sections of thalamic areas had no tdT^+ cell counts, except for vLGN, confirming our previous conclusion that cFosTRAP2; Ai14 may not be an optimal model for examining activity patterns in the sensory thalamus (Mesik et al., 2024).

Visual cortices show a reduction in active cell density followed by a partial rebound

We first examined the changes in tdT^+ cell density in V1 following visual deprivation (Fig. 3). We found that both DE and EN produced a statistically significant decrease in the tdT^+ cell density at 2 d (2dDE and 2dEN) followed by a partial rebound after 7 d (Fig. 3*B*). To qualitatively determine the tdT^+ cell density changes as a function of the depth from pia, we normalized the fraction of labeled cells per depth from pia to the median density of tdT^+ cells for each experimental group (Fig. 3*C*). This revealed that the density changes were happening largely in the superficial depths (100–400 µm from pia). To evaluate whether the changes were uniform across the depth of the cortex, we compared the relative fraction of tdT^+ cells at different depths from pia between the groups (Fig. 3*D*). We found a statistically significant decrease in the fraction of tdT^+ cells in the superficial depths (~100 µm from pia for DE groups and 200 µm depth for EN groups) corresponding to upper L2/3 and a relative increase in the tdT^+ cells at a deeper depth (~600 µm from pia for both DE and EN) which roughly corresponds to L5. This suggests that the initial decrease in active cell density is largely driven by a disproportionally greater decrease in the superficial layers. The relative distributions of tdT^+ cells in 2dDE and 7dDE groups were largely similar in the superficial depth suggesting that the rebound in active cell density with longer duration DE is relatively dampened in the superficial layers. In contrast, 7dEN recovered the relative proportion of active cells in the superficial layers (200–400 µm depth), which suggests that the rebound activation of superficial layers is more prominent with this more severe mode of visual deprivation. Collectively these results suggest that both modes of visual deprivation cause an initial decrease in active cells, more prominently in the superficial layers, which is followed by a more notable partial rebound with EN compared with DE.

A similar adaptation was observed in the secondary visual cortical areas (Fig. 4), which we grouped into two categories: lateral (V2L; Fig. 4*A–D*) and medial (V2M; Fig. 4*E–H*). There was a decrease in tdT^+ cell density following 2 d of DE or EN followed by a partial rebound at 7 d (Fig. 4*B*,*F*). The difference was statistically significant for V2L and only observed as a trend in V2M. Similar to what we observed in V1, most of the density changes occur in the superficial depths (100–400 µm from pia; Fig. 4*C*,*G*). When looking at the relative fractions of tdT^+ cells across the depths, 2 d of visual deprivation caused a relative shift from

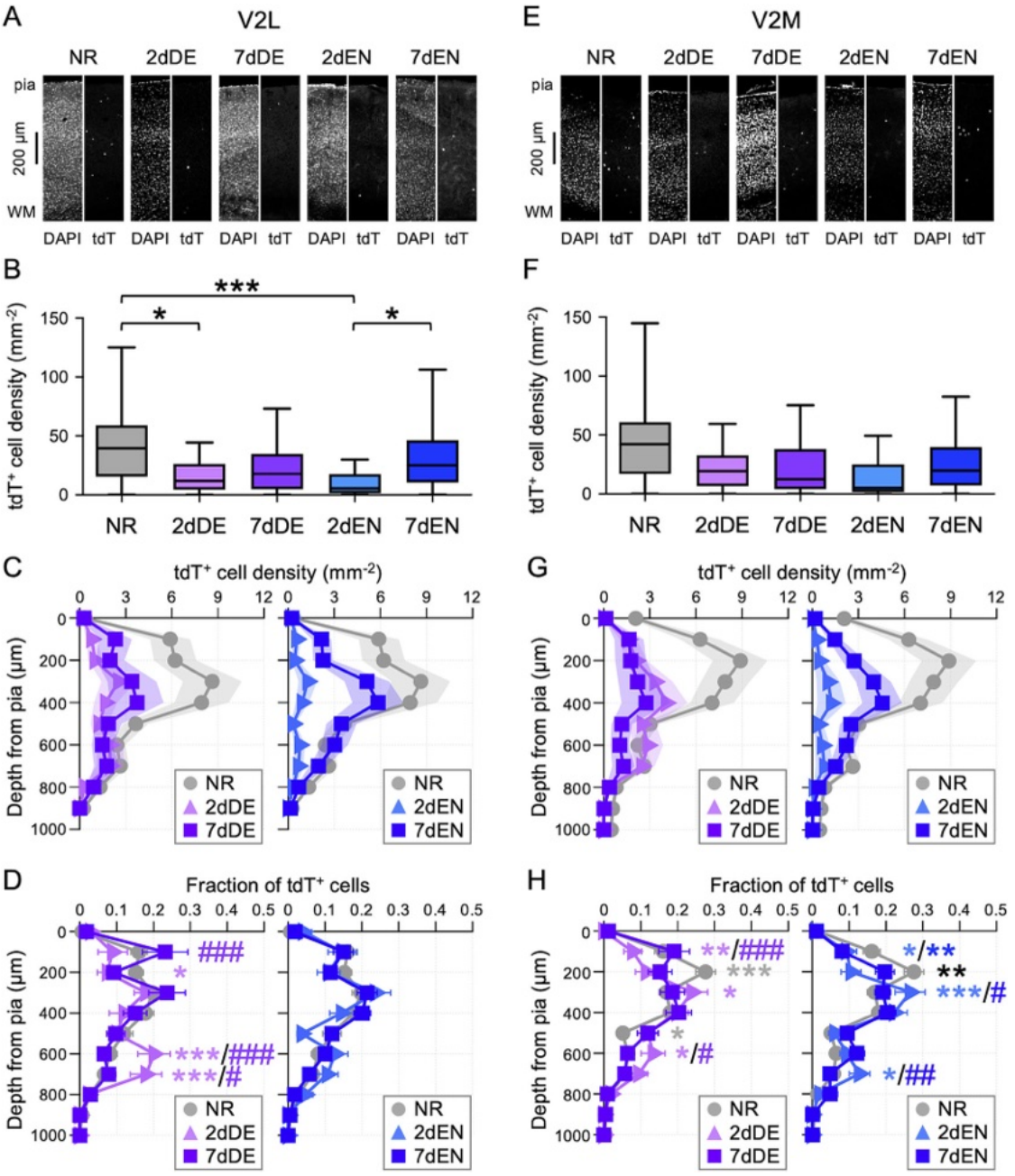

Figure 4. Secondary visual areas show a reduction in tdT$^+$ cells with a relatively larger decrease in the superficial depths after visual deprivation with a partial rebound. ***A–D***, Results from the lateral visual areas (V2L), which include VISl (visual area, lateral), VISal (visual area, anterolateral), and VISrl (visual area, rostrolateral) areas of the Allen Brain Atlas. ***E–H***, Results from the medial visual areas (V2M), which include VISa (visual area, anterior), VISam (visual area, anteromedial), and VISpm (visual area, posteromedial) of the Allen Brain Atlas. ***A***, ***E***, Example images of V2L (panel ***A***) and V2M (panel ***E***) sections across groups. Both DAPI and tdT images are shown side by side as labeled for NR, 2dDE, 7dDE, 2dEN, and 7dEN. Tiled confocal images taken at 10× were cropped and rotated to align the pia and WM for display. ***B***, ***F***, Quantification of tdT$^+$ cell density in V2L (panel ***B***) and V2M (panel ***F***) displayed as box and whisker plots. For V2L, median value (IQR): NR = 39.3 (IQR 15.9–58.7) mm^{-2}, $n = 52$ sections from six mice; 2dDE = 11.8 (IQR 4.5–25.4) mm^{-2}, $n = 29$ sections from five mice; 7dDE = 17.7 (IQR 5.2–34.4) mm^{-2}, $n = 28$ sections from five mice; 2dEN = 5.4 (IQR 1.4–15.5) mm^{-2}, $n = 51$ sections from seven mice; 7dEN = 25.0 (IQR 11.4–45.3) mm^{-2}, $n = 60$ sections from nine mice. LME model no-parametric one-way ANOVA test (ARTool): $F_{(4,26.919)} = 3.5455$, $p = 0.019$. Pairwise-comparisons post hoc test: *$p < 0.05$ and ***$p < 0.005$. For V2 M, median value (IQR): NR = 42.3 (IQR 17.7–59.3) mm^{-2}, $n = 57$ sections from six mice; 2dDE = 19.3 (IQR 7.5–30.9) mm^{-2}, $n = 33$ sections from six mice; 7dDE = 12.4 (IQR 4.5–38.0) mm^{-2}, $n = 32$ sections from five mice; 2dEN = 5.1 (IQR 1.7–24.6) mm^{-2}, $n = 62$ sections from seven mice; 7dEN = 19.7 (IQR 7.5–30.5) mm^{-2}, $n = 64$ sections from nine mice. LME model nonparametric one-way ANOVA test (ARTool): $F_{(4,28.011)} = 1.9356$, $p = 0.132$. ***C***, ***G***, The depth profile of tdT$^+$ cell density in each group normalized to the respective median density shown in panels ***B*** (for V2L) and ***F*** (for V2M). Shaded areas outline 95% confidence intervals. Left graphs, Comparison of NR, 2dDE, and 7dDE groups. Right graph, Comparison of NR, 2dEN, and 7dEN groups. ***D***, ***H***, Relative fraction of tdT$^+$ cells across the depth of V2L (panel ***D***) and V2M (panel ***H***). Left graphs (purple symbols), Comparison of NR, 2dDE, and 7dDE. For V2L (panel ***D***), two-way ANOVA: Interaction between group and depth, $F_{(24,1495)} = 2.709$, $p < 0.0001$. Tukey's multiple-comparisons post hoc test, * or $^{\#}p < 0.05$, *** or $^{\#\#\#}p < 0.005$ (light purple asterisks, between NR and 2dDE; dark purple hashtags, between 2dDE and 7dDE). For V2M (panel ***H***), two-way ANOVA: Interaction between group and depth, $F_{(24,1989)} = 3.718$, $p < 0.0001$. Tukey's multiple-comparisons post hoc test, * or $^{\#}p < 0.05$, **$p < 0.01$, *** or $^{\#\#\#}p < 0.005$ (light purple asterisks, between NR and 2dDE; dark purple hashtags, between 2dDE and 7dDE; light gray asterisks, NR is different from both 2dDE and 7dDE). Right graphs (blue symbols), Comparison of NR, 2dEN, and 7dEN. For V2L (panel ***D***), two-way ANOVA: Interaction between group and depth, $F_{(24,2275)} = 1.294$, $p = 0.1537$. For V2M (panel ***H***), two-way ANOVA: Interaction between group and depth, $F_{(20,2255)} = 4.636$, $p < 0.0001$. Tukey's multiple-comparisons post hoc test, * or $^{\#}p < 0.05$, ** or $^{\#\#}p < 0.01$, ***$p < 0.005$ (light blue asterisks, between NR and 2dEN; dark blue asterisks, between NR and 7dEN; dark blue hashtags, between 2dEN and 7dEN; black asterisks, all three groups are different from each other). Average ± SEM values are plotted. Symbols: NR, gray circles; 2dDE, light purple triangles; 7dDE, dark purple squares; 2dEN, light blue triangles; 7dEN, dark blue squares.

superficial to deeper depths, except for the V2L EN group which showed no change in the relative distribution at 2 or 7 d (Fig. 4*D*, *H*). With 7 d of visual deprivation, the relative shift in distribution was mostly normalized, except at ~200 µm depth where it stayed relatively low compared with NR. These results suggest that the secondary visual areas adapt very similarly to V1 while showing a potential difference in the degree of change between the lateral and medial areas with a more visible rebound with EN compared with DE.

Somatosensory cortical areas show minimal changes in the density of active neurons, except in the barrel fields

To determine whether visual deprivation leads to change in the activity of the somatosensory cortical areas, we examined tdT^+ cell density in the primary somatosensory cortex (S1), which were separately analyzed for the barrel fields (S1BF) and the other S1 areas (S1 other; Fig. 5), and the secondary somatosensory cortical area (S2; Fig. 6). We only observed a statistically significant difference in the tdT^+ cell density across the experimental groups in S1BF, where there was a decrease in density for 7dDE and 2dEN compared with the 7dEN group with pairwise post hoc analysis (Fig. 5*B*). This suggests an opposite trend of a change in the density of active cells between DE and EN, which was also evident when plotting the median density across the depths (Fig. 5*C*). The relative distribution of tdT^+ cells across the depth of S1BF did not significantly change for DE groups, but there was a statistically significant relative decrease at ~400 µm depth with 2 d of EN which normalized by 7 d (Fig. 5*D*). We observed similar trends in the other S1 areas (Fig. 5*E*,*F*) and S2 (Fig. 6*B*,*C*), which did not reach statistical significance.

Auditory cortical areas show a relative shift in the depth profile of active cells without overall changes in density

Next, we quantified tdT^+ cell density in the primary auditory (A1), dorsal auditory (AuD), and ventral auditory (AuV) cortical areas (Figs. 7, 8) and found no statistically significant change in the density of tdT^+ cells with both modes of visual deprivation (Figs. 7*B*, 8*B*,*F*). Qualitatively, there was a decrease in the median tdT^+ cell density around lower superficial layers (depth of 250–400 µm from pia) in A1 with visual deprivation (Fig. 7*C*) and a statistically significant decrease in a relative proportion of tdT^+ cells at ~300 µm depth (Fig. 7*D*). These results in A1 suggest that there is a persistent shift in the relative depth distribution of tdT^+ cells away from the superficial layer without significant changes in the overall density following both modes of visual deprivation.

Retrosplenial cortical areas did not show significant changes in the density of active cells

We also looked at the retrosplenial cortex (RSP) as an example of a multisensory cortical area and found no statistically significant change in the density of tdT^+ cells with visual deprivation. There was only a trend of a decrease with a longer duration of DE and an opposite trend with EN (Fig. 9). While there were qualitative changes in the median density of tdT^+ cells in the superficial depths (100–400 µm from pia), there was only a statistically significant increase in the relative proportion of tdT^+ cells at very superficial depth (~100 µm depth) with DE (Fig. 9*D*). These data suggest that there is minimal change in active cell density in this higher order multisensory cortical area with visual deprivation.

Changes in the sensory thalamic nuclei

Although cFosTRAP2 induction in the thalamus was quite minimal compared with the cortical areas (Fig. 2*C*), we found regulation with visual deprivation (Fig. 10). These results, however, should be taken with caution, because the number of detected cells in most sections is zero (Fig. 10*A*); hence even a slight misalignment of the delineated borders could lead to an apparent change in density, especially considering the small size of these thalamic nuclei. With such caveats in mind, we found that the density of tdT^+ cells in dLGN was reduced to zero in all sections examined with both visual deprivation paradigms (Fig. 10*B*), which is consistent with expectations. vLGN, which is largely GABAergic (Harrington, 1997; Inamura et al., 2011; Sabbagh et al., 2021) and is a target of intrinsically photosensitive retinal ganglion cells (ipRGCs; Hattar et al., 2002), had the highest basal level of cFosTRAP2 induction among the thalamic nuclei analyzed (Fig. 2*C*) and showed a trend of a decrease in the density of tdT^+ cells with visual deprivation (Fig. 10*C*). LP, a higher order visual thalamus equivalent to the pulvinar in higher mammals (Cortes et al., 2024), showed a time-dependent reduction in tdT^+ cell density with DE and an opposite trend with EN (Fig. 10*D*). Both the primary somatosensory thalamic nucleus (VPM; Fig. 10*E*) and the higher order somatosensory thalamic nucleus (PO; Fig. 10*F*) showed similar results, albeit differences in magnitude, where there were significant increases in tdT^+ cell density with visual deprivation, especially with 2dDE and 7dEN. There were barely any tdT^+ cells in the auditory thalamic nuclei in NR controls (Fig. 10*G*–*I*), but we observed a significant increase in the primary auditory thalamic nucleus (MGBv; Fig. 10*G*) with 7dEN and in one of the higher order auditory thalamic nuclei (MGBm; Fig. 10*I*) with both DE and EN. These results suggest that while cFosTRAP2 mice may not be the best model to examine activity changes in the thalamus, there is likely sufficient change in activity within these structures following visual deprivation that can be detected using this model.

Basic behavioral measures did not differ between DE and EN

To determine potential changes in behavior with visual deprivation, we monitored their behavior during an hour period to match the time of tamoxifen injection (ZT10~ZT12) for labeling active cells. Mice were imaged a day before visual deprivation by DE or EN and subsequently monitored 2 and 7 d afterward in their home cage. Behaviors in the darkroom were recorded under infrared light (950 nm) to avoid light exposure. Video recordings of the behavior were coded before being analyzed to prevent potential bias, and the duration of time spent for nine different behavioral categories was quantified for each mouse (Fig. 11*A*). Mice spent most of their time walking around or climbing the walls with greater time spent climbing after visual deprivation, which did not differ significantly between DE and EN (Fig. 11*B*). There was no statistically significant difference in percentage of time spent on any of the behavioral categories for DE and EN mice prior to and after visual deprivation (Fig. 11*B*), except for the social interaction category. DE mice were singly housed from the day before and during DE to mimic the condition used for the cFosTRAP2 labeling, which was done to allow weight measure of each mouse prior to DE needed for proper dosing of tamoxifen injections performed in the dark. In group-housed EN mice, ~10% of the time was spent on social interactions, which did not differ before (−1 d, NR) or after EN (Fig. 11*A*).

Considering the opposite direction of change in tdT^+ cell density in S1BF following DE and EN (Fig. 5*A*), we examined whether it could have resulted from the difference in social interactions. To do this, we repeated 7dDE with a cohort of group-housed cFosTRAP2;Ai14 mice (7dDEg). To distinguish each

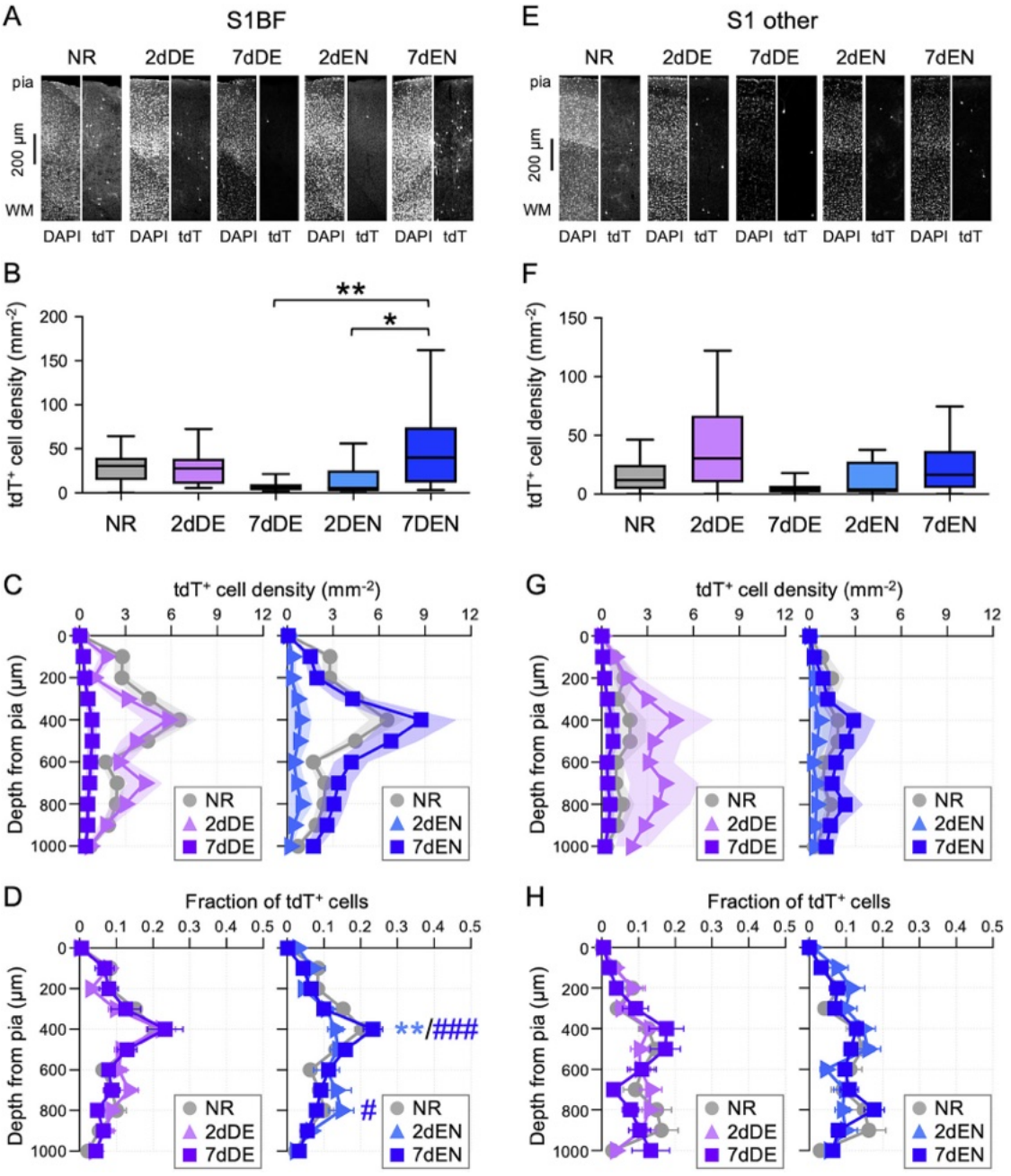

Figure 5. Differential changes in tdT + cell density with DE and EN in S1BF and a similar trend seen in S1 other areas. ***A*–*D***, Results from the primary somatosensory barrel cortex (S1BF). ***E*–*H***, Results from other S1 areas, which include SSp-ll (primary somatosensory area, lower limb), SSp-tr (primary somatosensory area, trunk), SSp-ul (primary somatosensory area, upper limb), SSp-*n* (primary somatosensory area, nose), and SSp-un (primary somatosensory area, unassigned) in the Allen Brain Atlas. ***A***, ***E***, Example images S1BF (panel ***A***) and S1 other, which corresponds to SSp-ll (panel ***E***) sections across groups. Both DAPI and tdT images are shown side by side as labeled for NR, 2dDE, 7dDE, 2dEN, and 7dEN. Tiled confocal images taken at 10× were cropped and rotated to align the pia and WM for display. ***B***, ***F***, Quantification of tdT$^+$ cell density in S1BF (panel ***B***) and S1 other (panel ***F***) displayed as box and whisker plots. For S1BF, median value (IQR): NR = 30.6 (IQR 15.2–39.2) mm^{-2}, $n = 35$ sections from six mice; 2dDE = 27.8 (IQR 10.3–36.1) mm^{-2}, $n = 26$ sections from six mice; 7dDE = 6.1 (IQR 2.9–9.0) mm^{-2}, $n = 25$ sections from five mice; 2dEN = 5.6 (IQR 1.7–25.6) mm^{-2}, $n = 41$ sections from seven mice; 7dEN = 40.0 (IQR 12.0–72.7) mm^{-2}, $n = 50$ sections from nine mice. LME model nonparametric one-way ANOVA test (ARTool): $F_{(4,28.00)} = 2.8400$, $p = 0.0428$. Pairwise-comparisons post hoc test: $^*p < 0.05$ and $^{***}p < 0.005$. For S1 other, median value (IQR): NR = 11.8 (IQR 5.8–24.0) mm^{-2}, $n = 17$ sections from five mice; 2dDE = 30.4 (IQR 10.1–65.8) mm^{-2}, $n = 18$ sections from six mice; 7dDE = 4.2 (IQR 1.6–5.9) mm^{-2}, $n = 17$ sections from five mice; 2dEN = 4.0 (IQR 1.6–24.8) mm^{-2}, $n = 22$ sections from six mice; 7dEN = 16.4 (IQR 5.3–36.6) mm^{-2}, $n = 23$ sections from nine mice. LME model nonparametric one-way ANOVA test (ARTool): $F_{(4,25.44)} = 1.778$, $p = 0.164$. ***C***, ***G***, The depth profile of tdT$^+$ cell density in each group normalized to the respective median density shown in panels ***B*** (for S1BF) and F (for S1 other). Shaded areas outline 95% confidence intervals. Left graphs, Comparison of NR, 2dDE, and 7dDE groups. Right graph, Comparison of NR, 2dEN, and 7dEN groups. ***D***, ***H***, Relative fraction of tdT$^+$ cells across the depth of S1BF (panel ***D***) and S1 other (panel ***H***). Left graphs (purple symbols), Comparison of NR, 2dDE, and 7dDE. For S1BF (panel ***D***), two-way ANOVA: Interaction between group and depth, $F_{(24,1092)} = 0.9309$, $p = 0.5592$. For S1 other (panel ***H***), two-way ANOVA: Interaction between group and depth, $F_{(24,1547)} = 1.332$, $p = 0.1305$. Right graphs (blue symbols), Comparison of NR, 2dEN, and 7dEN. For S1BF (panel ***D***), two-way ANOVA: Interaction between group and depth, $F_{(24,1378)} = 2.227$, $p = 0.0006$. Tukey's multiple-comparisons post hoc test, $^{\#}p < 0.05$, $^{**}p < 0.01$, $^{\#\#\#}p < 0.005$ (light blue asterisks, between NR and 2dEN; dark blue hashtags, between 2dEN and 7dEN). For S1 other (panel ***H***), two-way ANOVA: Interaction between group and depth, $F_{(24,2015)} = 1.330$, $p = 0.1307$. Average ± SEM values are plotted. Symbols: NR, gray circles; 2dDE, light purple triangles; 7dDE, dark purple squares; 2dEN, light blue triangles; 7dEN, dark blue squares.

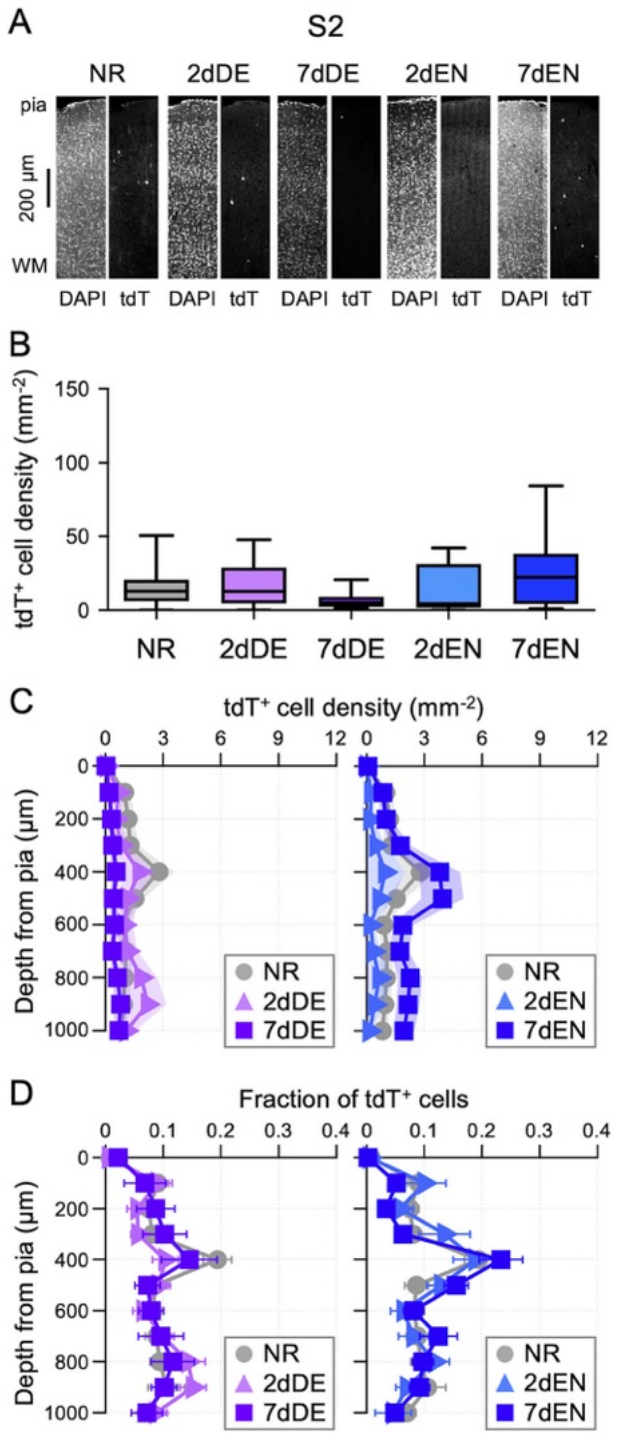

Figure 6. No significant changes in tdT$^+$ cell density or distribution across depth in S2. ***A***, Example images of S2, which correspond to SSs (somatosensory area, supplemental) in the Allen Brain Atlas, sections across groups. Both DAPI and tdT images are shown side by side as labeled for NR, 2dDE, 7dDE, 2dEN, and 7dEN. Tiled confocal images taken at 10× were cropped and rotated to align the pia and white matter (WM) for display. ***B***, Quantification of tdT$^+$ cell density in S2 across groups displayed as box and whisker plot. Median (IQR): NR = 12.9 (IQR 6.2–19.8) mm^{-2}, $n = 38$ sections from six mice; 2dDE = 12.8 (IQR 5.4–27.3) mm^{-2}, $n = 24$ sections from six mice; 7dDE = 5.2 (IQR 2.3–8.3) mm^{-2}, $n = 26$ sections from five mice; 2dEN = 4.3 (IQR 1.7–30.0) mm^{-2}, $n = 42$ sections from seven mice; 7dEN = 22.3 (IQR 4.1–36.7) mm^{-2}, $n = 46$ sections from nine mice. LME model one-way ANOVA test (ARTool): $F_{(4,27.96)} = 1.3040$, $p = 0.293$. ***C***, Depth profile of tdT$^+$ cell density in each group normalized to the respective median density shown in panel ***B***. Left graph, Comparison of NR, 2dDE, and 7dDE groups. Shaded areas outline 95% confidence intervals. Right graph, Comparison of NR, 2dEN, and 7dEN groups. ***D***, Relative fraction of tdT$^+$ cells across the depth of S2. Left graph, Comparison of NR, 2dDE, and 7dDE groups. Left graph, Comparison of NR, 2dDE, and 7dDE groups. Two-way ANOVA: Interaction between group and depth, $F_{(24,1092)} = 0.7296$, $p = 0.8245$. Right graph, Comparison of NR, 2dEN, and 7dEN groups. Two-way ANOVA: Interaction between group and depth, $F_{(24,1378)} = 1.106$, $p = 0.3280$. Average ± SEM values are plotted. Symbols: NR, gray circles; 2dDE, light purple triangles; 7dDE, dark purple squares; 2dEN, light blue triangles; 7dEN, dark blue squares.

mouse for the correct dosing of tamoxifen, we used commercial hair dye to apply patterns on the fur of mice, which allowed identification in the dark using infrared goggles. Another cohort of mice was also dyed and kept in the light for the same duration (NR). We found that the density of labeled tdT$^+$ cells in S1BF of 7dDEg was similar to what we observed for singly housed 7dDE (Fig. 11*C*) and the fraction of tdT$^+$ cells showed similar distribution across the cortical depth between NR and 7dDEg (Fig. 11*D*). These results suggest that the opposite changes seen in tdT$^+$ cell density in S1BF with DE and EN is not likely due to differences in housing conditions.

Discussion

Here we used cFosTRAP2;Ai14 mice to visualize the spatial profile of activity changes across various sensory cortical areas after adult-onset visual deprivation. The changes we observed are consistent with the idea of widespread cross-modal plasticity. In V1, we found an initial decrease in the density of active cells followed by a rebound increase, which suggests that there is delayed cross-modal recruitment by nonvisual inputs. A similar pattern was observed in the higher order visual cortical areas suggesting that cross-modal recruitment is not limited to V1. In the spared primary sensory cortical areas, we found changes in active cell density and/or redistribution across the depth of the cortex suggestive of compensatory plasticity. There was no significant or minimal change in the higher order cortical areas of the spared sensory modalities and in one of the multisensory areas examined. We also found evidence of activity changes in the sensory thalamic nuclei, which suggests that adaptation to vision loss is not restricted to the cortex. There was minimal change in basic behavior with visual deprivation.

The spatial extent of activity changes was examined based on cFos induction. IEGs, such as c-*fos*, are widely used to monitor activity changes in various brain areas (Barykina et al., 2022). It is pertinent to recognize that IEGs require a threshold or specific patterns of activity for robust induction. For c-*fos*, it is more effectively induced by rapidly repeated short bursts of stimuli than more sparsely repeated longer bursts (Sheng et al., 1993). Moreover, late-phase LTP (L-LTP) protocols, repeated trains of high-frequency stimulations, are effective at driving c-*fos* (Dragunow et al., 1989; Nikolaev et al., 1991; Kaczmarek, 1992). Therefore, our data should be interpreted in the context of such activity patterns rather than overall activity. We observed that visual areas have a higher density of tdT$^+$ cells compared with other sensory areas in NR controls and noted very low tdT expression in the sensory thalamic nuclei, except the vLGN (Fig. 2*C*). These results suggest that cFos induction under normal control conditions differ depending on the sensory modality and brain areas. Other studies have also noted that visual cortical neurons have higher basal activity compared with somatosensory and auditory cortices in rodents (Barth and Poulet, 2012). The lower tdT$^+$ cell density in thalamic nuclei could be due to activity patterns not meeting the conditions for cFos induction or tissue-specific regulation of c-*fos* promoter. It should be considered that the expression of tdT by cFosTRAP2 may not reflect the same

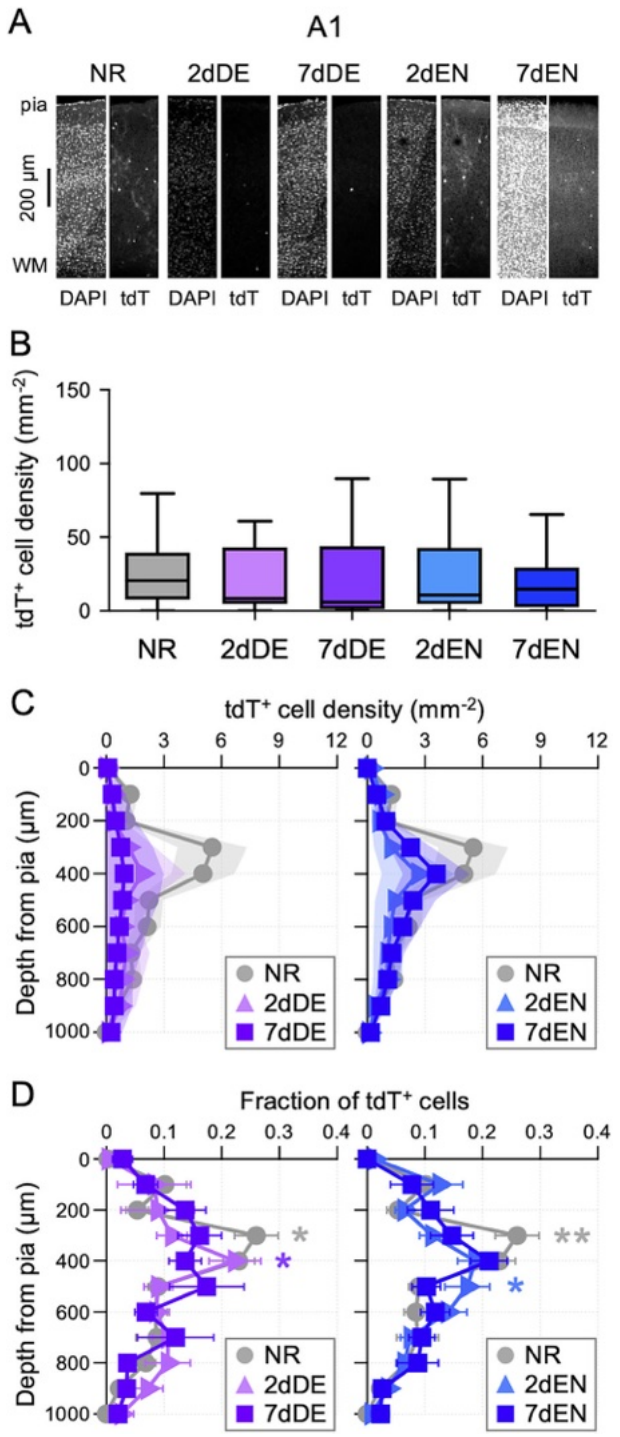

Figure 7. Visual deprivation does not significantly change the density of tdT$^+$ cells in A1 but shifts the distribution in depth. ***A***, Example images of A1, which corresponds to AUDp (primary auditory area) in the Allen Brain Atlas, sections across groups. Both DAPI and tdT images are shown side by side as labeled for NR, 2dDE, 7dDE, 2dEN, and 7dEN. Tiled confocal images taken at 10× were cropped and rotated to align the pia and white matter (WM) for display. ***B***, Quantification of tdT$^+$ cell density in A1 across groups displayed as Box and Whisker plot. Median (IQR): NR = 20.6 (IQR 9.5–38.1) mm^{-2}, $n = 33$ sections from six mice; 2dDE = 8.3 (IQR 4.9–38.7) mm^{-2}, $n = 18$ sections from four mice; 7dDE = 5.8 (IQR 2.1–40.8) mm^{-2}, $n = 19$ sections from five mice; 2dEN = 10.8 (IQR 4.8–41.3) mm^{-2}, $n = 42$ sections from seven mice; 7dEN = 14.8 (IQR 2.7–29.4) mm^{-2}, $n = 32$ sections from eight mice. LME model nonparametric one-way ANOVA test (ARTool): $F_{(4,24.81)} = 0.2169$, $p = 0.926$. ***C***, Depth profile of tdT$^+$ cell density in each group normalized to the respective median density shown in panel ***B***. Shaded areas outline 95% confidence intervals. Left graph, Comparison of NR, 2dDE, and 7dDE groups. Right graph, Comparison of NR, 2dEN, and 7dEN groups. ***D***, Relative fraction of tdT$^+$ cells across the depth of A1. Left graph, Comparison of NR, 2dDE, and 7dDE groups. Two-way ANOVA: Interaction between group and depth, $F_{(24,728)} = 1.589$, $p = 0.0369$. Tukey's multiple-comparisons post hoc test, $*p < 0.05$ (light purple asterisks, between NR and 2dDE; light gray asterisks, NR is different from both 2dDE and 7dDE). Right graph, Comparison of NR, 2dEN, and 7dEN groups. Two-way ANOVA: Interaction between group and depth, $F_{(24,1170)} = 1.672$, $p = 0.0223$. Tukey's multiple-comparisons post hoc test, $*p < 0.05$, $**p < 0.01$ (light blue asterisks, between NR and 2dEN; gray asterisks, NR different from 2dEN and 7dEN). Average ± SEM values are plotted. Symbols: NR, gray circles; 2dDE, light purple triangles; 7dDE, dark purple squares; 2dEN, light blue triangles; 7dEN, dark blue squares.

level of activity in the spared versus the deprived cortical areas. Following single whisker rearing, it was observed that cFos labeled neurons in the spared barrel have a higher action potential threshold than those in the deprived barrel within S1BF (Barth et al., 2004). Another consideration is that cFos is not restricted to a specific cell type. In the cortex, we found that tdT$^+$ expression is predominantly in neurons (Fig. 2*B*), but it is not restricted to a specific neuronal type. Indeed, we observed a high density of tdT$^+$ cells in vLGN, mainly composed of GABAergic neurons (Harrington, 1997). We also observed cell morphologies in the cortex that reflect excitatory neurons and GABAergic neurons (Figs. 1*H*, 2*B*). Changes in tdT$^+$ cell density should mostly reflect excitatory neurons since GABAergic neurons are ∼20% of the cortical neuronal population (Rudy et al., 2011). However, parvalbumin (PV)-positive neurons, in particular, have higher excitability and firing rates (Rudy et al., 2011) and hence could be over-represented in the tdT$^+$ cell counts. Even among excitatory neurons, those with higher basal activity may constitute a distinct population. For example, in V1 L4, neurons with a high basal firing rate display increased intrinsic excitability and receive stronger local recurrent excitatory synaptic drive (Trojanowski et al., 2021). Similarly, in S1BF, cFos-positive L2/3 neurons form a distinct functional network (Jouhanneau et al., 2014). In the hippocampus, high excitability neurons more likely partake in forming the memory engram network (Silva et al., 2009; Guskjolen and Cembrowski, 2023) with cFos-positive ensembles involved in memory generalization (Sun et al., 2020). The significance of tdT$^+$ cells labeled in our study will require further investigation, but here we found that the density and cortical depth profile of tdT$^+$ cells change reflecting widespread cross-modal plasticity.

Our main observation is that the visual cortical areas undergo an initial reduction in activity followed by a partial rebound (Figs. 3, 4), which contrasts with the complete loss of tdT$^+$ cells in dLGN (Fig. 10*B*). We previously reported that 2dDE and 7dDE result in the strengthening of lateral intracortical inputs in V1 L2/3 (Petrus et al., 2014, 2015; Chokshi et al., 2019). These findings suggest that potentiation of lateral intracortical synapses precedes neuronal activity rebound and activity through these potentiated inputs likely drives the rebound. Consistent with this, we saw a proportionally larger rebound at 200–400 µm depth from pia (Fig. 3*D*) corresponding to L2/3. Rebound activity in V1 is congruent with the idea of cross-modal recruitment of V1 by nonvisual inputs. There are similar findings with monocular enucleation, where the deprived V1 showed a rebound activation monitored by IEG *zif268* that was dependent on whisking activity (Van Brussel et al., 2011; Nys et al., 2014). These results are in line with studies from blind human subjects where V1 is activated by braille and speech (Sadato et al., 1996; Buchel et al., 1998; Roder et al., 2002; Bedny et al., 2015). Whether the rebound we observed

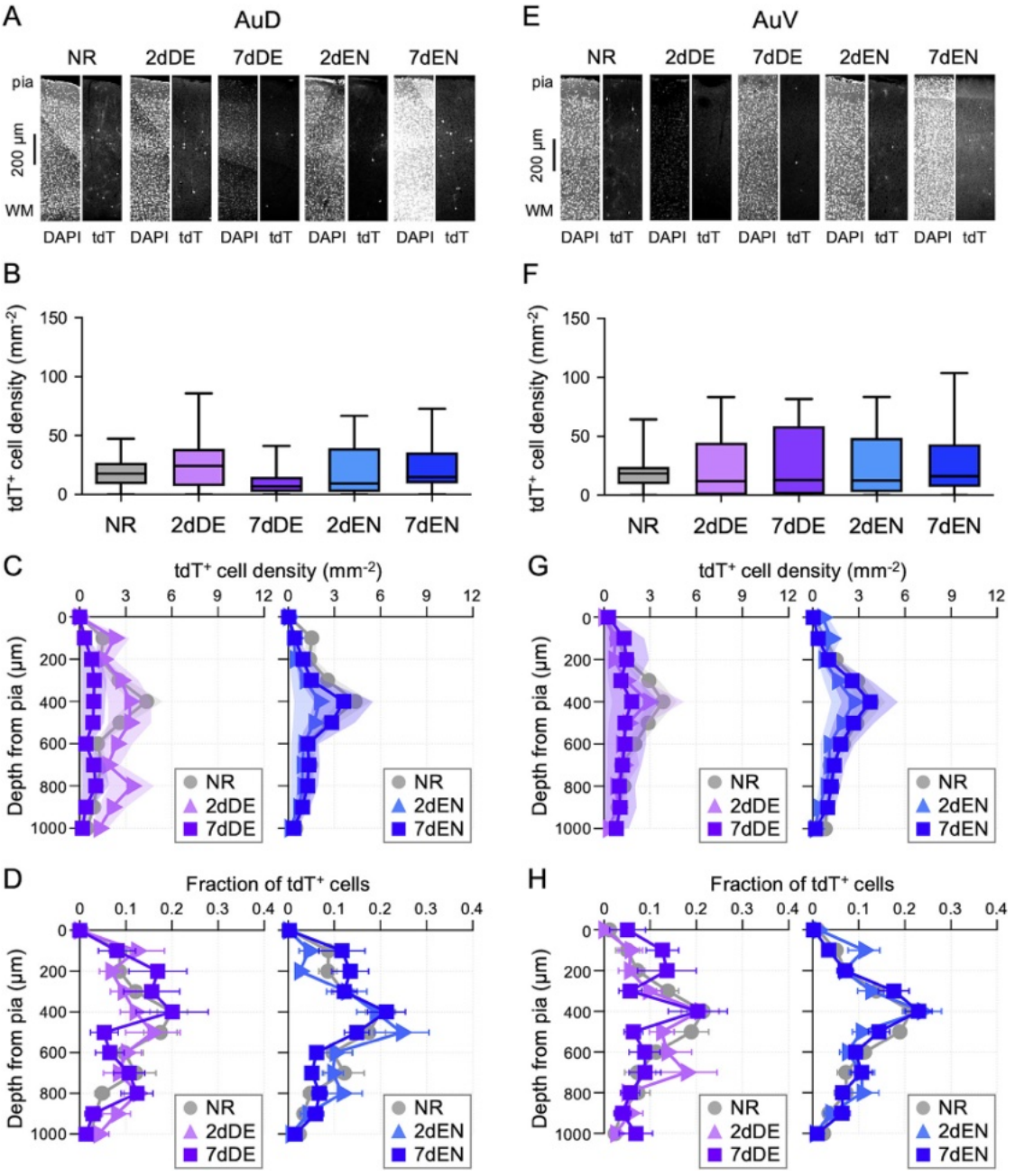

Figure 8. Visual deprivation does not alter the density or the depth profile of tdT$^+$ cells in secondary auditory areas. ***A***, ***E***, Example images from higher order auditory areas, AuD (panel ***A***) and AuV (panel ***E***), which correspond to AUDd (auditory area, dorsal) and AUDv (auditory area, ventral), respectively, in the Allen Brain Atlas. Both DAPI and tdT images are shown side by side as labeled for NR, 2dDE, 7dDE, 2dEN, and 7dEN. Tiled confocal images taken at 10× were cropped and rotated to align the pia and WM for display. ***B***, ***F***, Quantification of tdT$^+$ cell density in AuD (panel ***B***) and AuV (panel ***F***) displayed as box and whisker plots. For AuD, median value (IQR): NR = 17.6 (IQR 9.3–26.1) mm^{-2}, $n = 32$ sections from six mice; 2dDE = 24.2 (IQR 7.6–35.3) mm^{-2}, $n = 18$ sections from five mice; 7dDE = 6.8 (IQR 2.1–11.7) mm^{-2}, $n = 17$ sections from five mice; 2dEN = 9.3 (IQR 2.2–39.1) mm^{-2}, $n = 33$ sections from seven mice; 7dEN = 14.7 (IQR 9.3–34.6) mm^{-2}, $n = 29$ sections from eight mice. LME model nonparametric one-way ANOVA test (ARTool): $F_{(4,25.89)} = 0.5107$, $p = 0.728$. For AuV, median value (IQR): NR = 18.5 (IQR 9.3–23.7) mm^{-2}, $n = 44$ sections from six mice; 2dDE = 11.8 (IQR 0–40.5) mm^{-2}, $n = 29$ sections from five mice; 7dDE = 12.8 (IQR 2.2–54.4) mm^{-2}, $n = 20$ sections from five mice; 2dEN = 12.4 (IQR 2.7–48.1) mm^{-2}, $n = 51$ sections from seven mice; 7dEN = 16.1 (IQR 7.3–41.9) mm^{-2}, $n = 44$ sections from eight mice. LME model nonparametric one-way ANOVA test (ARTool): $F_{(4,26.09)} = 0.2726$, $p = 0.893$. ***C***, ***G***, The depth profile of tdT$^+$ cell density in each group normalized to the respective median density shown in panels ***B*** (for AuD) and ***F*** (for AuV). Shaded areas outline 95% confidence intervals. Left graphs, Comparison of NR, 2dDE, and 7dDE groups. Right graph, Comparison of NR, 2dEN, and 7dEN groups. ***D***, ***H***, Relative fraction of tdT$^+$ cells across the depth of AuD (panel ***D***) and AuV (panel ***H***). Left graphs (purple symbols), Comparison of NR, 2dDE, and 7dDE. For AuD (panel ***D***), two-way ANOVA: Interaction between group and depth, $F_{(24,741)} = 1.162$, $p = 0.2699$. For AuV (panel ***H***), two-way ANOVA: Interaction between group and depth, $F_{(24,949)} = 1.363$, $p = 0.1144$. Right graphs (blue symbols), Comparison of NR, 2dEN, and 7dEN. For AuD (panel ***D***), two-way ANOVA: Interaction between group and depth, $F_{(24,1040)} = 1.206$, $p = 0.2258$. For AuV (panel ***H***), two-way ANOVA: Interaction between group and depth, $F_{(24,1560)} = 1.069$, $p = 0.3730$. Average ± SEM values are plotted. Symbols: NR, gray circles; 2dDE, light purple triangles; 7dDE, dark purple squares; 2dEN, light blue triangles; 7dEN, dark blue squares.

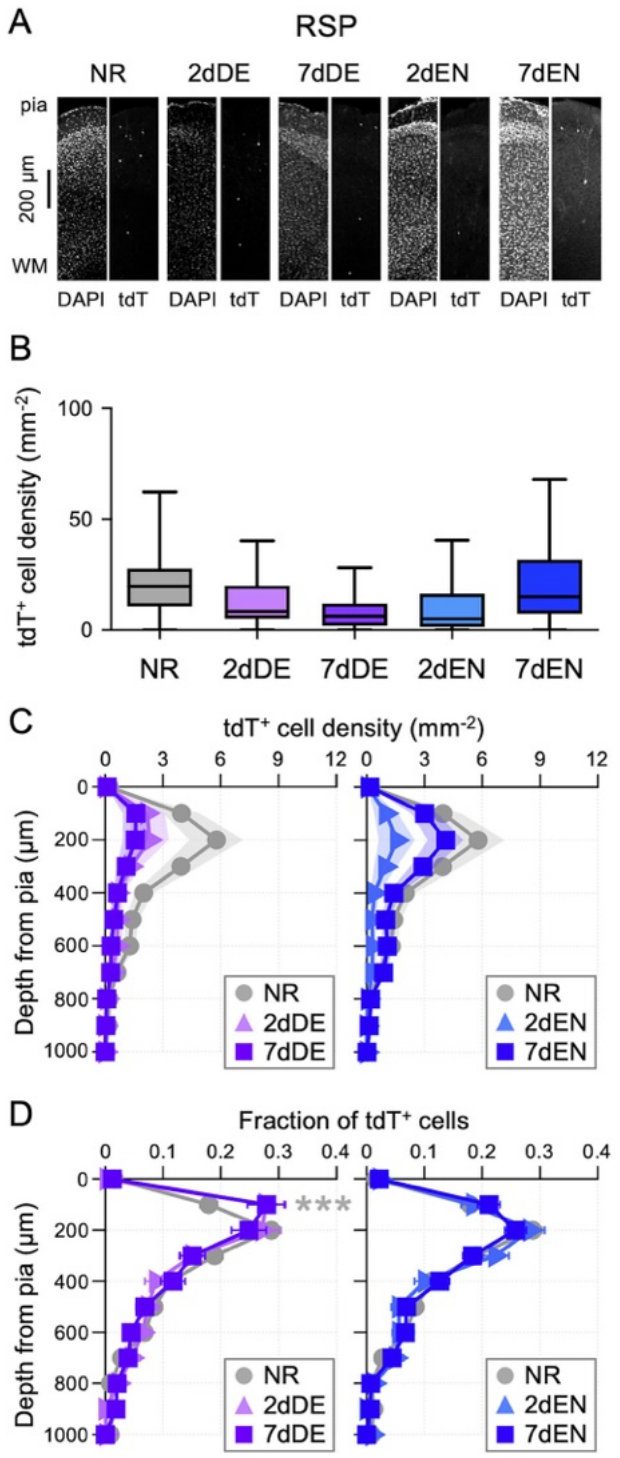

Figure 9. No significant change in the density of tdT$^+$ cells in RSP with visual deprivation. ***A***, Example images of RSP sections, which include RSPv (retrosplenial area, ventral), RSPd (retrosplenial area, dorsal), and RSPagl (retrosplenial area, lateral agranular) areas in the Allen Brain Atlas. Both DAPI and tdT images are shown side by side as labeled for NR, 2dDE, 7dDE, 2dEN, and 7dEN. Tiled confocal images taken at 10× were cropped and rotated to align the pia and white matter (WM) for display. ***B***, Quantification of tdT$^+$ cell density in RSP across groups displayed as box and whisker plot. Median (IQR): NR = 19.7 (IQR 10.7–27.1) mm^{-2}, $n = 69$ sections from six mice; 2dDE = 8.3 (IQR 5.6–19.0) mm^{-2}, $n = 38$ sections from five mice; 7dDE = 6.2 (IQR 2.5–11.8) mm^{-2}, $n = 37$ sections from five mice; 2dEN = 5.0 (IQR 1.5–15.9) mm^{-2}, $n = 67$ sections from seven mice; 7dEN = 15.0 (IQR 7.4–31.0) mm^{-2}, $n = 78$ sections from nine mice. LME model nonparametric one-way ANOVA test (ARTool): $F_{(4,27.07)} = 1.8040$, $p = 0.157$. ***C***, Depth profile of tdT$^+$ cell density in each group normalized to the respective median density shown in panel ***B***. Shaded areas outline 95% confidence intervals. Left graph, Comparison of NR, 2dDE, and 7dDE groups. Right graph, Comparison of NR, 2dEN, and 7dEN groups. ***D***, Relative fraction of tdT$^+$ cells across the depth of RSP. Left graph, Comparison of NR, 2dDE, and 7dDE groups. Two-way ANOVA: Interaction between group and depth, $F_{(24,4745)} = 2.324$, $p = 0.0003$. Tukey's multiple-comparisons post hoc test, ***$p < 0.005$ (light gray asterisks, NR is different from both 2dDE and 7dDE). Right graph, Comparison of NR, 2dEN, and 7dEN groups. Two-way ANOVA: Interaction between group and depth, $F_{(24,6162)} = 0.9448$, $p = 0$. 5390. Average ± SEM values are plotted. Average ± SEM values are plotted. Symbols: NR, gray circles; 2dDE, light purple triangles; 7dDE, dark purple squares; 2dEN, light blue triangles; 7dEN.

here is due to recruitment of V1 by spared sensory modalities will require follow-up studies. We noted a trend of an increase in tdT$^+$ cell density in LP with visual deprivation, which may be explained by it receiving input from multisensory areas in addition to visual areas (Bennett et al., 2019; Cortes et al., 2024). The rebound activity in V2 areas is only significant in V2L and observed as a trend in V2M (Fig. 4) suggesting that they may be part of a different functional circuitry. Indeed, V2L tends to respond better to higher temporal frequency, while V2M prefers higher spatial frequency, visual stimuli (Marshel et al., 2011). Furthermore, V2M, but not V2L, is considered part of the default mode network (DMN) in rodents, which includes RSP (Lu et al., 2012; Whitesell et al., 2021). We found a similar trend in tdT$^+$ cell density in RSP (Fig. 9) as seen in V2M supporting the idea that their activity may be correlated from being part of the DMN.

In the spared sensory areas, we found differences in adaptation that support the notion of compensatory plasticity (Ewall et al., 2021). In S1BF, we observed opposing regulation of tdT$^+$ cell density where DE trended to decrease while EN showed an initial decrease followed by a rebound (Fig. 5*A*). This was somewhat mirrored in the somatosensory thalamus where both VPM and PO showed a similar pattern (Fig. 10*E*,*F*), which suggests an increase in activity propagated through the thalamus. The increase in thalamic activity could potentially support the potentiation of feedforward synapses from L4 to L2/3 seen after 2 d visual deprivation (Jitsuki et al., 2011). A longer duration of visual deprivation results in a decrease in miniature excitatory postsynaptic current (mEPSC) amplitude in S1BF L2/3 neurons (Goel et al., 2006; He et al., 2012), which is likely an adaptation to increased feedforward activity (Ewall et al., 2021; Lee, 2023). Collectively, these results support a model where S1BF undergoes compensatory plasticity upon DE by an increase in feedforward activity through the somatosensory thalamus driving potentiation of feedforward synapses and a delayed homeostatic depression of intracortical inputs to reduce the activity level in S1BF. The opposite trend seen with EN could suggest that the potentiation of the S1BF feedforward circuit might be more prominent with this more extreme mode of vision loss. Unlike S1BF, A1 undergoes a much subtle change with visual deprivation, where there was no significant change in the overall density of active cells but a significant shift away from superficial depths (Fig. 7). The reduction in active cells in the superficial layers is consistent with prior observations showing refinement of intracortical connectivity within A1 L2/3 and L4 (Meng et al., 2015, 2017), as well as sparsification of sound encoding in L2/3 (Solarana et al., 2019) following 7dDE. We also reported that 7dDE potentiates thalamocortical inputs from MGBv to L4 and from L4 to L2/3 (Petrus et al., 2014, 2015) and disinhibition of MGBv (Whitt et al., 2022). Here, we observed a significant increase in the relative fraction of tdT$^+$ cells in the depth of 400–450 µm (Fig. 7*D*), which could reflect the potentiation of thalamocortical

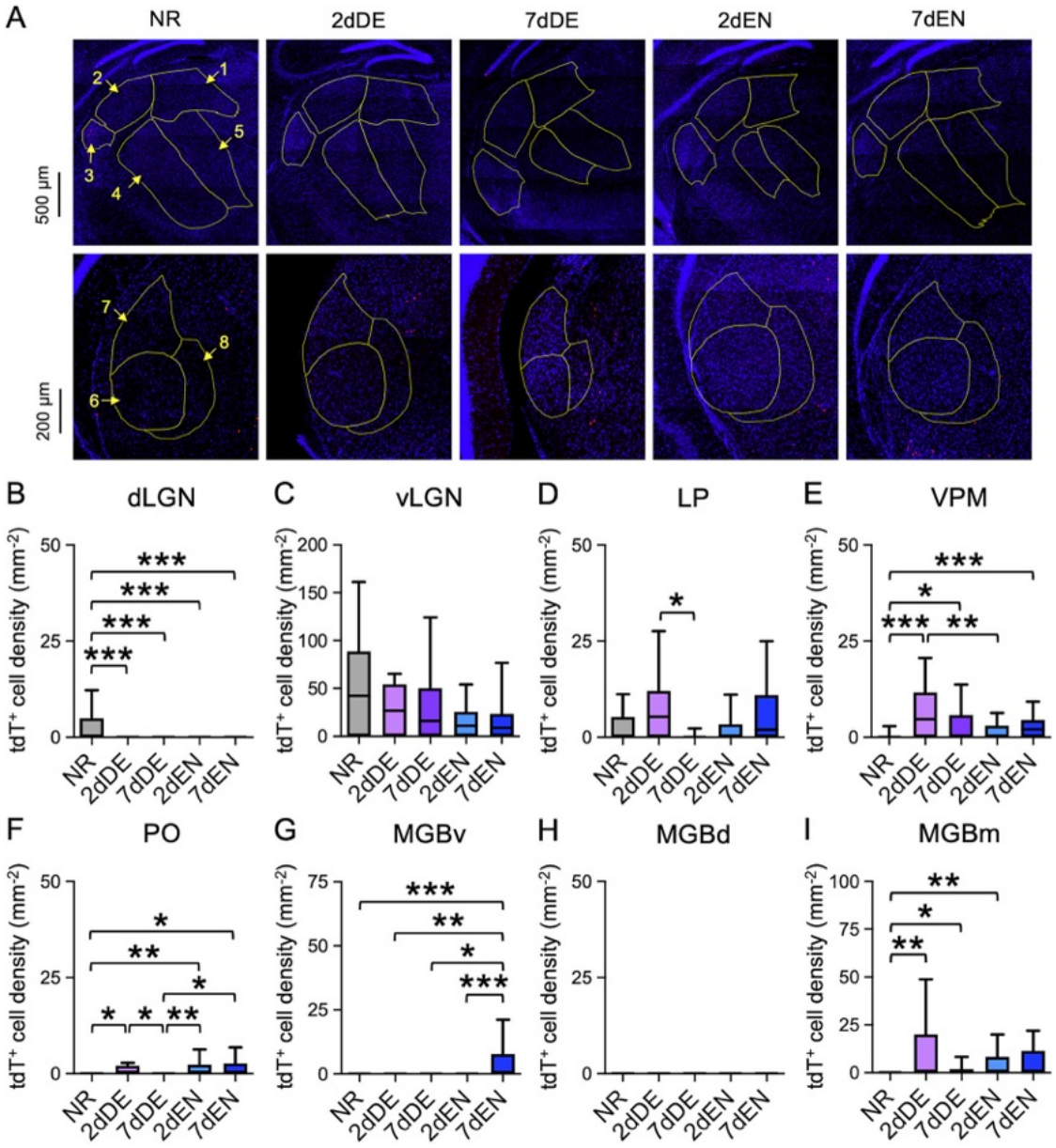

Figure 10. Comparison of tdT$^+$ cell density across the sensory thalamic nuclei. ***A***, Examples of tiled scanned images of DAPI (blue) and tdT (red) channels overlaid. Top panels, Anterior sections containing LP (1), dLGN (2), vLGN (3), VPM (4), and PO (5). Bottom panels, Posterior sections containing MGBv (6), MGBd (7), and MGBm (8). Yellow outlines are the borders of each area based on a template matching to the Allen Brain Atlas using the DAPI channel (see Materials and Methods for details). ***B***, Quantification of tdT$^+$ cell density in dLGN across groups displayed in a box and whisker plot. Median value with IQR in parentheses: NR = 0 (IQR 0–4.63) mm^{-2}, $n = 38$ sections from six mice; 2dDE = 0 (IQR 0–0) mm^{-2}, $n = 18$ sections from five mice; 7dDE = 0 (IQR 0–0) mm^{-2}, $n = 20$ sections from five mice; 2dEN = 0 (IQR 0–0) mm^{-2}, $n = 33$ sections from seven mice; 7dEN = 0 (IQR 0–0) mm^{-2}, $n = 30$ sections from eight mice. LME model nonparametric one-way ANOVA test (ARTool): $F_{(4,22.075)} = 9.666$, $p = 0.0001$. Pairwise-comparisons post hoc test: ***$p < 0.005$. ***C***, Quantification of tdT$^+$ cell density in vLGN across groups displayed in a box and whisker plot. Median value with IQR in parentheses: NR = 42.3 (IQR 0–87.8) mm^{-2}, $n = 39$ sections from six mice; 2dDE = 26.7 (IQR 0–53.5) mm^{-2}, $n = 21$ sections from six mice; 7dDE = 16.1 (IQR 0–47.3) mm^{-2}, $n = 23$ sections from five mice; 2dEN = 11.0 (IQR 0.9–23.2) mm^{-2}, $n = 38$ sections from seven mice; 7dEN = 8.8 (IQR 0–19.8) mm^{-2}, $n = 36$ sections from nine mice. LME model nonparametric one-way ANOVA test (ARTool): $F_{(4,25.702)} = 1.597$, $p = 0.2052$. ***D***, Quantification of tdT$^+$ cell density in LP across groups displayed in a box and whisker plot. Median value with IQR in parentheses: NR = 0 (IQR 0–4.3) mm^{-2}, $n = 44$ sections from six mice; 2dDE = 5.3 (IQR 0–11.8) mm^{-2}, $n = 25$ sections from six mice; 7dDE = 0 (IQR 0–0) mm^{-2}, $n = 21$ sections from five mice; 2dEN = 0 (IQR 0–3.2) mm^{-2}, $n = 47$ sections from seven mice; 7dEN = 2.0 (IQR 0–10.7) mm^{-2}, $n = 51$ sections from nine mice. LME model nonparametric one-way ANOVA test (ARTool): $F_{(4,27.735)} = 3.189$, $p = 0.0001$. Pairwise-comparisons post hoc test: *$p < 0.05$. ***E***, Quantification of tdT$^+$ cell density in VPM across groups displayed in a box and whisker plot. Median value with IQR in parentheses: NR = 0 (IQR 0–0) mm^{-2}, $n = 26$ sections from six mice; 2dDE = 4.7 (IQR 0.4–10.4) mm^{-2}, $n = 18$ sections from six mice; 7dDE = 0 (IQR 0–5.2) mm^{-2}, $n = 22$ sections from five mice; 2dEN = 0 (IQR 0–2.1) mm^{-2}, $n = 24$ sections from seven mice; 7dEN = 2.0 (IQR 0–3.6) mm^{-2}, $n = 29$ sections from nine mice. LME model nonparametric one-way ANOVA test (ARTool): $F_{(4,23.668)} = 4.913$, $p = 0.005$. Pairwise-comparisons post hoc test: *$p < 0.05$, **$p < 0.01$, ***$p < 0.005$. ***F***, Quantification of tdT$^+$ cell density in PO across groups displayed in a box and whisker plot. Median value with IQR in parentheses: NR = 0 (IQR 0–0) mm^{-2}, $n = 24$ sections from six mice; 2dDE = 0 (IQR 0–1.9) mm^{-2}, $n = 17$ sections from six mice; 7dDE = 0 (IQR 0–0) mm^{-2}, $n = 18$ sections from five mice; 2dEN = 0 (IQR 0–2.3) mm^{-2}, $n = 28$ sections from seven mice; 7dEN = 0 (IQR 0–2.4) mm^{-2}, $n = 30$ sections from eight mice. LME model nonparametric one-way ANOVA test (ARTool): $F_{(4,23.163)} = 4.194$, $p = 0.011$. Pairwise-comparisons post hoc test: *$p < 0.05$, **$p < 0.01$. ***G***, Quantification of tdT$^+$ cell density in MGBv across groups displayed as box and whisker plot. Median value with IQR in parentheses: NR = 0 (IQR 0–0) mm^{-2}, $n = 16$ sections from six mice; 2dDE = 0 (IQR 0–0) mm^{-2}, $n = 9$ sections from four mice; 7dDE = 0 (IQR 0–0) mm^{-2}, $n = 8$ sections from three mice; 2dEN = 0 (IQR 0–0) mm^{-2}, $n = 26$ sections from seven mice; 7dEN = 0 (IQR 0–7.5) mm^{-2}, $n = 28$ sections from nine mice. LME model nonparametric one-way ANOVA test (ARTool): $F_{(4,21.963)} = 5.492$, $p = 0.003$. Pairwise-comparisons post hoc test: *$p < 0.05$, **$p < 0.01$, ***$p < 0.005$. ***H***, Quantification of tdT$^+$ cell density in MGBd across groups displayed as box and whisker plot. Median value with IQR in parentheses: NR = 0 (IQR 0–0) mm^{-2}, $n = 16$ sections from six mice; 2dDE = 0 (IQR 0–0) mm^{-2}, $n = 11$ sections from four mice; 7dDE = 0 (IQR 0–0) mm^{-2}, $n = 9$ sections from three mice; 2dEN = 0 (IQR 0–0) mm^{-2}, $n = 25$ sections from seven mice; 7dEN = 0 (IQR 0–0) mm^{-2}, $n = 23$ sections

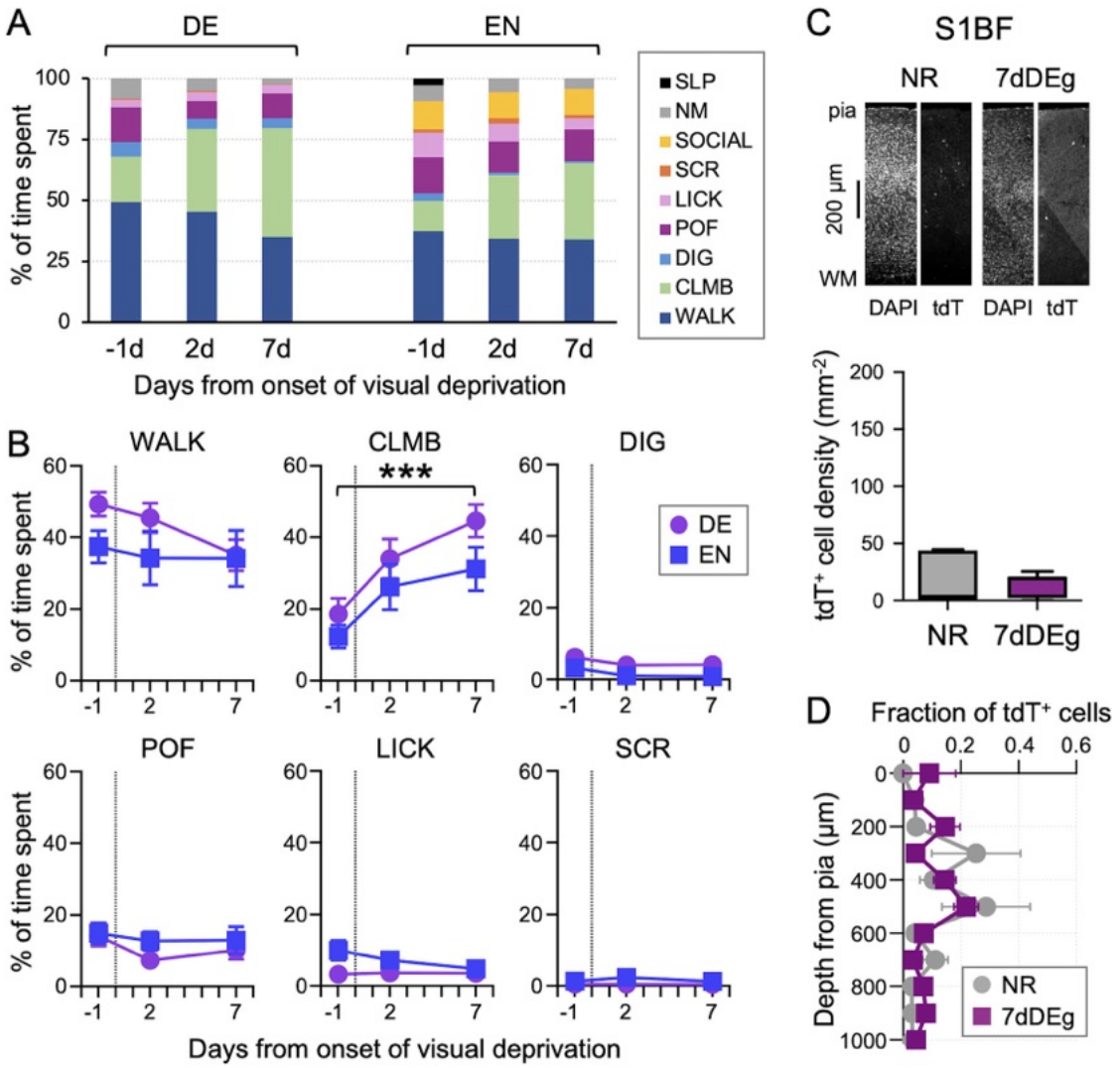

Figure 11. Comparison of basic behavior before and after visual deprivation. ***A***, Quantification of percentage (%) of time spent in nine different behavioral categories at 1 d before (−1 d, NR) and subsequently at 2 and 7 d after the onset of visual deprivation (DE and EN). Video recordings were done between ZT10 and ZT12 for 1 h. Behavioral categories (listed in order from bottom to top as displayed in the fraction bar graph): walking around (WALK), wall climbing (CLMB), digging the bedding (DIG), front paw on face (POF), licking itself (LICK), scratching with back paw (SCR), social interactions (SOCIAL), not moving (NM), and sleeping (SLP). DE: 9 mice (4 males and 5 females), EN: 8 mice (4 males and 4 females). Mice in the DE group lack the social interaction category because they were singly housed from −1 d onward (see Materials and Methods for details). % of time spent in social interactions for the EN group did not differ across the days: −1dEN (NR) = 11.8 ± 0.81%, 2dEN = 10.7 ± 1.92%, 7dEN = 10.7 ± 2.66%; repeated-measures one-way ANOVA, $F_{(2,14)} = 0.1103$, $p = 0.8963$. ***B***, Statistical comparison of % of time spent in each category between DE and EN conditions. Only six of the major categories are graphed for display. The dotted vertical line denotes day 0, which is when visual deprivation was initiated. Two-way ANOVA interaction between the duration and the mode of visual deprivation (DE, purple circles; EN, blue squares): WALK: $F_{(2,30)} = 0.8265$, $p = 0.4473$; CLMB: $F_{(2,30)} = 0,3571$, $p = 0.7026$; DIG: $F_{(2,30)} = 0.01476$, $p = 0.9854$; POF: $F_{(2,30)} = 0.3546$, $p = 0.7044$; LICK: $F_{(2,30)} = 2.177$, $p = 0.1309$; SCR: $F_{(2,30)} = 1.648$, $p = 0.2093$. For CLMB category, the duration of visual deprivation was identified as a significant source of variation: $F_{(1.878,28.17)} = 13.19$, $p = 0.0001$ (denoted as ***). ***C***, Top, Example images of S1BF sections from NR and DE mice group housed (7dDEg). Both DAPI and tdT images are shown side by side. Tiled confocal images taken a 10× were cropped and rotated to align the pia and WM for display. Bottom, Quantification of tdT^+ cell density in S1BF displayed as a box and whisker plot (NR, 6 sections from 2 mice; 7dDEg, 11 sections from 3 mice). LME model nonparametric one-way ANOVA test (ARTool): $F_{(1,3.062)} = 0.0314$, $p = 0.8704$. ***D***, Comparison of the relative fraction of tdT^+ cells across the depth of S1BF between NR (gray circles) and 7dDEg (plum squares). Two-way ANOVA: Interaction between group and depth, $F_{(10,150)} = 1.302$, $p = 0.2341$.

inputs to A1 L4 and support reduced sound detection threshold in these neurons (Petrus et al., 2014). However, we only observed marginal changes in MGBv that could reflect disinhibition (Fig. 10*G*), which may be due to very low cFosTRAP2 induction in the auditory thalamus (Fig. 2*C*). Overall, our results support a widespread change in activity profile across various sensory areas with adult-onset visual deprivation consistent with large-scale cross-modal adaptation.

←

from seven mice. LME model nonparametric one-way ANOVA test (ARTool): $F_{(4,17.004)} = 2.430$, $p = 0.088$. ***I***, Quantification of tdT^+ cell density in MGBm across groups displayed in a box and whisker plot. Median value with IQR in parentheses: NR = 0 (IQR 0–0) mm^{-2}, $n = 18$ sections from six mice; 2dDE = 0 (IQR 0–19.5) mm^{-2}, $n = 15$ sections from four mice; 7dDE = 0 (IQR 0–0) mm^{-2}, $n = 10$ sections from three mice; 2dEN = 0 (IQR 0–7.8) mm^{-2}, $n = 26$ sections from seven mice; 7dEN = 0 (IQR 0–0) mm^{-2}, $n = 25$ sections from eight mice. LME model nonparametric one-way ANOVA test (ARTool): $F_{(4,17.362)} = 3.286$, $p = 0.036$. Pairwise-comparisons post hoc test: *$p < 0.05$, **$p < 0.01$.

References

Bankhead P, et al. (2017) Qupath: open source software for digital pathology image analysis. Sci Rep 7:16878.

Barth AL, Gerkin RC, Dean KL (2004) Alteration of neuronal firing properties after in vivo experience in a FosGFP transgenic mouse. J Neurosci 24: 6466–6475.

Barth AL, Poulet JF (2012) Experimental evidence for sparse firing in the neocortex. Trends Neurosci 35:345–355.

Barykina NV, Karasev MM, Verkhusha VV, Shcherbakova DM (2022) Technologies for large-scale mapping of functional neural circuits active during a user-defined time window. Prog Neurobiol 216:102290.

Bavelier D, Neville HJ (2002) Cross-modal plasticity: where and how? Nat Rev Neurosci 3:443–452.

Bedny M, Richardson H, Saxe R (2015) "Visual" cortex responds to spoken language in blind children. J Neurosci 35:11674–11681.

Bennett C, Gale SD, Garrett ME, Newton ML, Callaway EM, Murphy GJ, Olsen SR (2019) Higher-order thalamic circuits channel parallel streams of visual information in mice. Neuron 102:477–492.e5.

Buchel C, Price C, Frackowiak RS, Friston K (1998) Different activation patterns in the visual cortex of late and congenitally blind subjects. Brain 121: 409–419.

Chokshi V, Gao M, Grier BD, Owens A, Wang H, Worley PF, Lee HK (2019) Input-specific metaplasticity in the visual cortex requires Homer1a-mediated mGluR5 signaling. Neuron 104:736–748.e6.

Cortes N, Ladret HJ, Abbas-Farishta R, Casanova C (2024) The pulvinar as a hub of visual processing and cortical integration. Trends Neurosci 47: 120–134.

DeNardo LA, Liu CD, Allen WE, Adams EL, Friedmann D, Fu L, Guenthner CJ, Tessier-Lavigne M, Luo L (2019) Temporal evolution of cortical ensembles promoting remote memory retrieval. Nat Neurosci 22:460–469.

Dragunow M, Abraham WC, Goulding M, Mason SE, Robertson HA, Faull RL (1989) Long-term potentiation and the induction of c-fos mRNA and proteins in the dentate gyrus of unanesthetized rats. Neurosci Lett 101:274–280.

Elbert T, Sterr A, Rockstroh B, Pantev C, Muller MM, Taub E (2002) Expansion of the tonotopic area in the auditory cortex of the blind. J Neurosci 22:9941–9944.

Ewall G, Parkins S, Lin A, Jaoui Y, Lee H-K (2021) Cortical and subcortical circuits for cross-modal plasticity induced by loss of vision. Front Neural Circuits 15:665009.

Flavell SW, Greenberg ME (2008) Signaling mechanisms linking neuronal activity to gene expression and plasticity of the nervous system. Annu Rev Neurosci 31:563–590.

Friard O, Gamba M (2016) BORIS: a free, versatile open-source event-logging software for video/audio coding and live observations. Methods Ecol Evol 7:1325–1330.

Goel A, Jiang B, Xu LW, Song L, Kirkwood A, Lee HK (2006) Cross-modal regulation of synaptic AMPA receptors in primary sensory cortices by visual experience. Nat Neurosci 9:1001–1003.

Guskjolen A, Cembrowski MS (2023) Engram neurons: encoding, consolidation, retrieval, and forgetting of memory. Mol Psychiatry 28:3207–3219.

Harrington ME (1997) The ventral lateral geniculate nucleus and the intergeniculate leaflet: interrelated structures in the visual and circadian systems. Neurosci Biobehav Rev 21:705–727.

Hattar S, Liao HW, Takao M, Berson DM, Yau KW (2002) Melanopsin-containing retinal ganglion cells: architecture, projections, and intrinsic photosensitivity. Science 295:1065–1070.

He K, Petrus E, Gammon N, Lee HK (2012) Distinct sensory requirements for unimodal and cross-modal homeostatic synaptic plasticity. J Neurosci 32: 8469–8474.

Huber E, Chang K, Alvarez I, Hundle A, Bridge H, Fine I (2019) Early blindness shapes cortical representations of auditory frequency within auditory cortex. J Neurosci 39:5143–5152.

Inamura N, Ono K, Takebayashi H, Zalc B, Ikenaka K (2011) Olig2 lineage cells generate GABAergic neurons in the prethalamic nuclei, including the zona incerta, ventral lateral geniculate nucleus and reticular thalamic nucleus. Dev Neurosci 33:118–129.

Jitsuki S, et al. (2011) Serotonin mediates cross-modal reorganization of cortical circuits. Neuron 69:780–792.

Jouhanneau JS, Ferrarese L, Estebanez L, Audette NJ, Brecht M, Barth AL, Poulet JF (2014) Cortical fosGFP expression reveals broad receptive field excitatory neurons targeted by POm. Neuron 84:1065–1078.

Kaczmarek L (1992) Expression of c-fos and other genes encoding transcription factors in long-term potentiation. Behav Neural Biol 57:263–266.

Lazzerini Ospri L, Prusky G, Hattar S (2017) Mood, the circadian system, and melanopsin retinal ganglion cells. Annu Rev Neurosci 40:539–556.

Lee HK (2023) Metaplasticity framework for cross-modal synaptic plasticity in adults. Front Synaptic Neurosci 14:1087042.

Lu H, Zou Q, Gu H, Raichle ME, Stein EA, Yang Y (2012) Rat brains also have a default mode network. Proc Natl Acad Sci U S A 109:3979–3984.

Marshel JH, Garrett ME, Nauhaus I, Callaway EM (2011) Functional specialization of seven mouse visual cortical areas. Neuron 72:1040–1054.

Meng X, Kao JP, Lee HK, Kanold PO (2015) Visual deprivation causes refinement of intracortical circuits in the auditory cortex. Cell Rep 12: 955–964.

Meng X, Kao JP, Lee HK, Kanold PO (2017) Intracortical circuits in thalamorecipient layers of auditory cortex refine after visual deprivation. eNeuro 4:ENEURO.0092-17.2017.

Merabet LB, Hamilton R, Schlaug G, Swisher JD, Kiriakopoulos ET, Pitskel NB, Kauffman T, Pascual-Leone A (2008) Rapid and reversible recruitment of early visual cortex for touch. PLoS One 3:e3046.

Mesik L, et al. (2024) Transcranial low-intensity focused ultrasound stimulation of the visual thalamus produces long-term depression of thalamocortical synapses in the adult visual cortex. J Neurosci 44: e0784232024.

Mesik L, Lee HK (2023) Cross-modal plasticity of cortical and thalamic circuits. In: *The cerebral cortex and thalamus* (Usrey WM, Sherman SM, eds), pp 573–582. New York, USA: Oxford University Press.

Nikolaev E, Tischmeyer W, Krug M, Matthies H, Kaczmarek L (1991) c-fos protooncogene expression in rat hippocampus and entorhinal cortex following tetanic stimulation of the perforant path. Brain Res 560: 346–349.

Nys J, Aerts J, Ytebrouck E, Vreysen S, Laeremans A, Arckens L (2014) The cross-modal aspect of mouse visual cortex plasticity induced by monocular enucleation is age dependent. J Comp Neurol 522:950–970.

Park WJ, Fine I (2024) A unified model for cross-modal plasticity and skill acquisition. Front Neurosci 18:1334283.

Pascual-Leone A, Torres F (1993) Plasticity of the sensorimotor cortex representation of the reading finger in Braille readers. Brain 116:39–52.

Paxinos G, Franklin KBJ (2001) *The mouse brain in streotaxic coordinates*, Ed 3. San Diego, USA: Academic Press.

Petrus E, Isaiah A, Jones AP, Li D, Wang H, Lee HK, Kanold PO (2014) Crossmodal induction of thalamocortical potentiation leads to enhanced information processing in the auditory cortex. Neuron 81:664–673.

Petrus E, Rodriguez G, Patterson R, Connor B, Kanold PO, Lee HK (2015) Vision loss shifts the balance of feedforward and intracortical circuits in opposite directions in mouse primary auditory and visual cortices. J Neurosci 35:8790–8801.

Roder B, Stock O, Bien S, Neville H, Rosler F (2002) Speech processing activates visual cortex in congenitally blind humans. Eur J Neurosci 16:930–936.

Rodriguez G, Chakraborty D, Schrode KM, Saha R, Uribe I, Lauer AM, Lee HK (2018) Cross-modal reinstatement of thalamocortical plasticity accelerates ocular dominance plasticity in adult mice. Cell Rep 24:3433–3440.e4.

Rudy B, Fishell G, Lee S, Hjerling-Leffler J (2011) Three groups of interneurons account for nearly 100% of neocortical GABAergic neurons. Dev Neurobiol 71:45–61.

Sabbagh U, Govindaiah G, Somaiya RD, Ha RV, Wei JC, Guido W, Fox MA (2021) Diverse GABAergic neurons organize into subtype-specific sublaminae in the ventral lateral geniculate nucleus. J Neurochem 159: 479–497.

Sadato N, Pascual-Leone A, Grafman J, Ibanez V, Deiber MP, Dold G, Hallett M (1996) Activation of the primary visual cortex by Braille reading in blind subjects. Nature 380:526–528.

Schindelin J, et al. (2012) Fiji: an open-source platform for biological-image analysis. Nat Methods 9:676–682.

Sheng HZ, Fields RD, Nelson PG (1993) Specific regulation of immediate early genes by patterned neuronal activity. J Neurosci Res 35:459–467.

Silva AJ, Zhou Y, Rogerson T, Shobe J, Balaji J (2009) Molecular and cellular approaches to memory allocation in neural circuits. Science 326:391–395.

Solarana K, Liu J, Bowen Z, Lee HK, Kanold PO (2019) Temporary visual deprivation causes decorrelation of spatiotemporal population responses in adult mouse auditory cortex. eNeuro 6:ENEURO.0269-19.2019.

Sun X, Bernstein MJ, Meng M, Rao S, Sorensen AT, Yao L, Zhang X, Anikeeva PO, Lin Y (2020) Functionally distinct neuronal ensembles within the memory engram. Cell 181:410–423.e7.

Trojanowski NF, Bottorff J, Turrigiano GG (2021) Activity labeling in vivo using CaMPARI2 reveals intrinsic and synaptic differences between neurons with high and low firing rate set points. Neuron 109:663–676.e5.

Van Brussel L, Gerits A, Arckens L (2011) Evidence for cross-modal plasticity in adult mouse visual cortex following monocular enucleation. Cereb cortex 21:2133–2146.

Whitesell JD, et al. (2021) Regional, layer, and cell-type-specific connectivity of the mouse default mode network. Neuron 109:545–559.e8.

Whitt JL, Ewall G, Chakraborty D, Adegbesan A, Lee R, Kanold PO, Lee HK (2022) Visual deprivation selectively reduces thalamic reticular nucleus-mediated inhibition of the auditory thalamus in adults. J Neurosci 42: 7921–7930.

Wobbrock JO, Findlater L, Gergle D, Higgins JJ (2011) The aligned rank transform for nonparametric factorial analyses using only ANOVA procedures. In: *Proceedings of the SIGCHI conference on human factors in computing systems (CHI ' 11)* (Tan D, ed), pp 143–146. New York: ACM Press.